Novel approach of the graphene nanolubricant for energy saving via anti-friction/wear in automobile engines

Mohamed Kamal Ahmed Ali[a,b,c], Hou Xianjun[a,c,*], Mohamed A.A. Abdelkareem[a,b,c], M. Gulzar[d], A.H. Elsheikh[e]

[a] Hubei Key Laboratory of Advanced Technology for Automotive Components, Wuhan University of Technology, Wuhan, 430070, China
[b] Automotive and Tractors Engineering Department, Faculty of Engineering, Minia University, El-Minia, 61111, Egypt
[c] Hubei Collaborative Innovation Center for Automotive Components Technology, Wuhan, 430070, China
[d] Department of Mechanical Engineering, Khwaja Fareed University of Engineering and Information Technology, Rahim Yar Khan, Pakistan
[e] Department of Production Engineering and Mechanical Design, Tanta University, Tanta, 31527, Egypt

ARTICLE INFO

ABSTRACT

The friction and wear of the worn surfaces is a principal cause of energy dissipation in automobile engines. Therefore, the objective of this work was to improve the tribological behavior using graphene (Gr) nanolubricant designed for saving energy and reducing the exhaust emissions. Anti-friction and anti-wear properties of Gr nanolubricant have been evaluated using tribometer based on ASTMG181. Herein, we present the self-healing mechanism responsible for the tribological events. To link tribological tests with factual engine performance, the engine performance was evaluated utilizing AVL dynamometer under New European Driving Cycle (NEDC). The tribological results showed that the lubrication via Gr nanolubricant improves the anti-friction and anti-wear properties by 29–35% and 22–29%, respectively, during boundary lubrication system. The engine lubrication using Gr nanolubricant revealed reducing cumulative fuel mass consumed by 17% with road load simulation during NEDC test. Furthermore, the exhaust emissions (CO, CO_2, HC and NOx) were decreased by 2.79–5.42%, as compared to the reference oil.

1. Introduction

The lube oils industry is continually studying new technology to improve engine performance [1]. Ultra-thin Gr as nano-additives have been widely used recently in different fields and applications such as nano-tribology and nanofluids in automobiles. Gr consists of carbon atoms as a 0.335 nm sheet thickness [2]. What makes the Gr attractive and worthy of being used as nanolubricant additives is the very small size of the diameters ranging from 1-100 nm, which it can easily fill the protrusions of the sliding contact interfaces in mechanical systems [3]. The friction and wear of the worn surfaces is a principal cause of energy dissipation in automobile engines [4]. Total power generated by the engine is reduced in the range 17–19% because of the frictional losses. Existing and future automotive engines would require more efficient engine oils. Therefore, the investigations on energy saving via anti-friction/wear have gained tremendous attention as a promising direction in the performance of automobile engines [1,5]. Furthermore, the distribution of oil supply generally does not coincide with where the demand is located. Therefore, many countries import oil at an unprecedented scale, which can lead to not balance between trade and national security challenges. It is reported that we could save as much as US$ 120 billion per year because of the frictional power in engines and rolling resistance reduction in automobile [6,7]. Additionally, new efficiency and emission standards imposed on vehicles have been the main driving force behind the development of cleaner and more fuel-efficient lubricants over the years. That is to say, the world needs novel strategies in which our sources of energy are affordable, accessible and sustainable. The current study supports that goal using Gr nano-sheets as nanolubricants.

The controlling friction via the use of nano-additives leads to anti-friction and anti-wear, which achieve fuel economy in automobile engines [8]. In the tribological results by Ali et al. [9], Al_2O_3/TiO_2 were added to engine oil (5W-30) as friction and wear modifiers with a grain size of 8–12 nm, showing a friction reduction of 50% and the wear rate of the piston ring enhanced by 40% compared with the base oil results. Another study by Rasheed et al. [10] indicated that, for API 20W-50 SN/CF mixed with Gr nano-sheets (0.01 wt.%, 12 nm thickness), the friction coefficient of the piston ring/liner assembly dropped to 21%

Table 1
Survey of the tribological performance of nanomaterials as additives in the lubricants.

| No.	Year	Ref.	Nanolubricant Details				Tribometer	Conditions			Reduction	
			Nanomaterials	Grain Size	Concentration	Base Oil		Load	Speed	Temperature	Wear %	Friction %
1.	2016	[10]	Gr	12 nm (thickness)	0.01 wt%	API 20W-50	4-ball tribometer	40 N	1200 rpm	75 °C	18%	21%
2.	2012	[14]	Ag-MoS$_2$	Ag < 100 nm MoS$_2$ 3–5 μm	2 wt.%	Formulated Oil[a]	Pin-on-disk	5 N	0.13–16 cm/s	RT[b]	30-37%	15-20%
3.	2014	[15]	OFMs	N/A	0.5 wt.%	5W-20	Ball-on-disc	30 N	0.1 m/s	100 °C	5%	10%
4.	2016	[11]	Al$_2$O$_3$ TiO$_2$	8-12 nm 10 nm	0.25 wt.%	5W-30	Piston ring/cylinder liner	120N	0.5 m/s	100 °C	21% 29%	45% 50%
5.	2015	[16]	Carbon-Fe Nanocapsules (CFNCs)	20-100 nm	0.07 wt.%	Mineral oil	Block-on-ring	650N	1.65 m/s	RT	27.8%	8%
9.	2015	[17]	g-C$_3$N$_4$/Cu	20 nm	0.5 wt.%	Paraffin base oil	Ball-on-disc	20 N	100 rpm	RT	65%	33%
10.	2018	[18]	Ni-MoS$_2$	2 μm (MoS$_2$) 3 μm (Ni)	0.5 wt.%	SN 500 mineral oil	Four ball wear tester	392.4 N	1200 rpm	75 °C	41%	21%
11.	2018	[19]	MoS$_2$	250 nm	0.25 wt.%	ISO VG 32	Block-on-ring	326N	1 m/s	RT	34.3%	28.6%
12.	2017	[20]	Gr Oxide (GrO)	18 μm (width)	0.04 wt.%	500 SN base oil	Four-ball machine	147N	1200 rpm	N/A	37%	33%
13.	2017	[21]	MoS$_2$	305.3 nm	2 wt.%	MACs[c]	Reciprocating UMT – 2MT sliding tester	20 N	300 rpm	RT	80%	40%
14.	2018	[22]	Cu	10-30 nm	3 wt.%	Mineral ester base oils	Pin-on-disk and Four-ball tester	392N	1200 rpm	40 °C 100 °C	64%	60% 40%
15.	2018	[23]	TiO$_2$	20 nm	4 wt.%	Water based oil	Ball-on-disk	5 N	50 mm/s	RT	34%	20%
16.	2017	[24]	Sc-Au/GrO	10-90nm	0.10 wt.%	Neat PAO6 oil	Ball-on-disk	10N	0.1 m/s	RT	72.8%	33.6%
17	2015	[25]	Gr	–	0.05 wt%	Palm Oil	Four ball wear tester	80kg	1200 rpm	RT	16.2%	7%
18.	2010	[26]	Ni20	20 nm	0.5 wt.%	PAO6	Block-on-ring	165N	2 m/s	N/A	45%	30%
19.	2008	[27]	Cu	20 nm	1 wt.%	SN 650	Ring/Disc interface	50-200 N	1.51 m/s	RT	67.4%	18.3%
20.	2013	[28]	TiO$_2$	20-25 nm	0.25 wt.%	Base oil (mineral oil).	Reciprocating	14.7 N	0.05 m/s	RT	N/A	21%
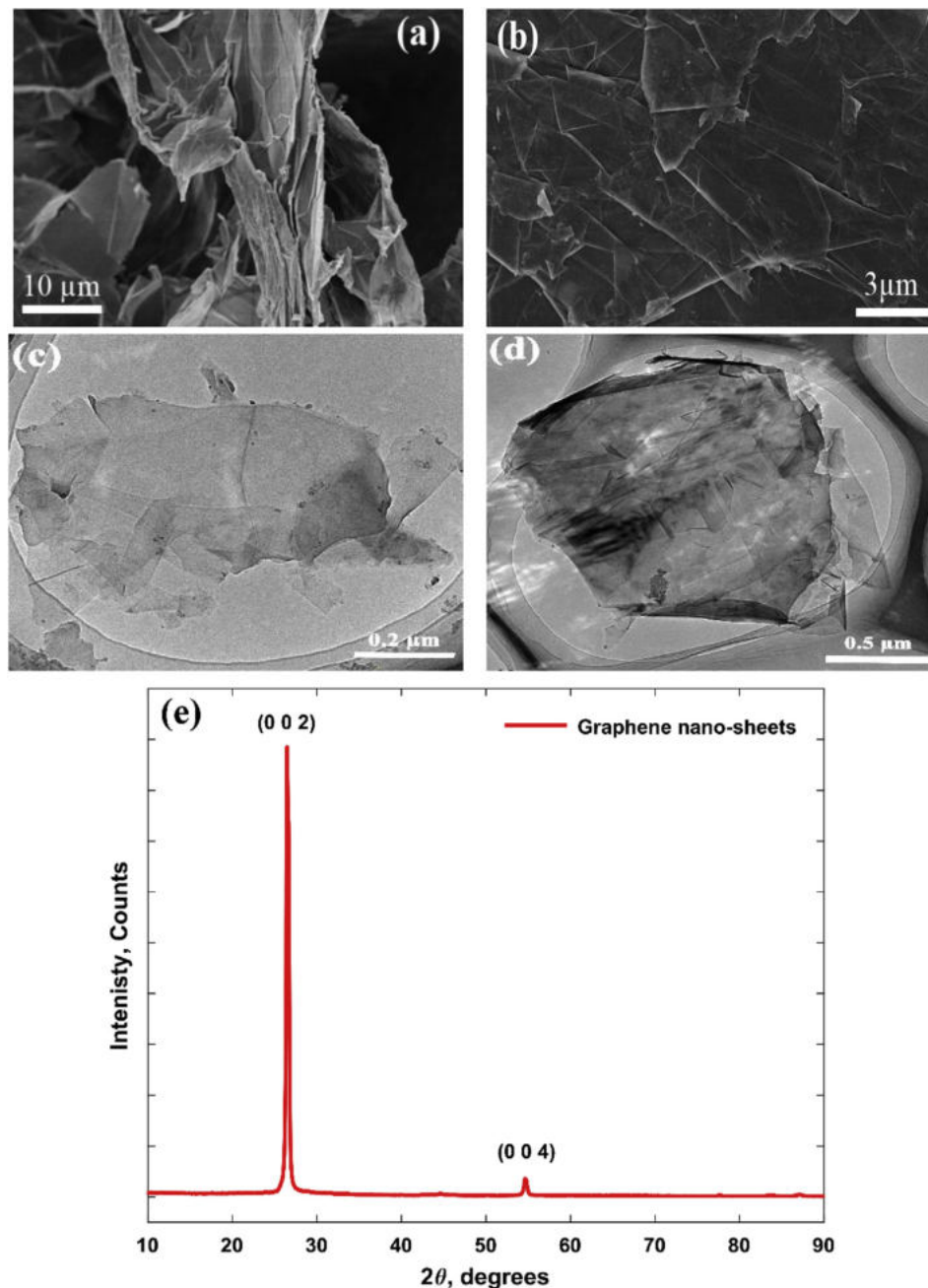
Fig. 1. Microscopic morphology and characterization of Gr nano-sheets. (a, b) SEM images of Gr nano-sheets, (c, d) TEM images of Gr nano-sheets (e) XRD patterns of the Gr nanostructures.

Table 2
Gr nano-sheets specifications.

Parameter	Value
Diameter	5-10 μm
Thickness	3-10 nm
Specific Surface Area	31.657 m^2/g
Tap Density	0.075 g/cm^3
Apparent Density	0.050 g/cm^3
Carbon Content	> 99.5%

lower than its value in the base oil case and the wear rate enhanced by 18% when the test conditions were 40 N load, 1200 rpm speed and temperature of 75 °C. Additionally, the results also showed that using Gr nanolubricant in internal combustion engines enhanced the heat transfer by 70% and thermal conductivity by 23%. Table 1 supplies an up-to-date survey of laboratory studies addressing the tribological performance of lubricants with nanomaterial additives. It is observed that nano-additives have the potentials of significantly reduce the friction and wear trends regards high performing lubricants at different operating conditions [11–13].

In recent experimental studies regarding nanolubricant, Ali et al. [1], the fuel consumption of a petrol engine has been improved by 16–20% using Al_2O_3/TiO_2 nanolubricant for New European Driving Cycle (NEDC) and different conditions. Whereas, in Ref. [29], 1–5% of fuel saving was achieved when the engine was lubricated by MoS_2 nanolubricant at different conditions. Skjoedt et al. [30] investigated the effects of friction modifier and replacing viscosity grade on engine friction. The results indicated that the fuel economy improvement by 0.9–2.6% using molybdenum dithiocarbamate (MoDTC). Tormos et al.
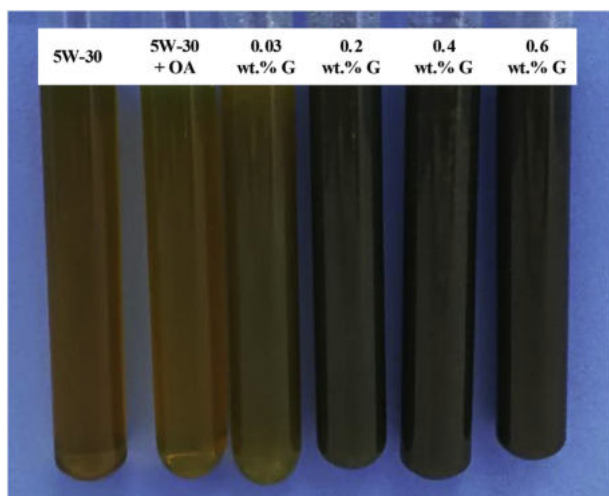
Fig. 2. Digital photography of a reference oil (5W-30) and Gr nanolubricant samples.

[31] studied the effect of the use of low viscosity engine oils on fuel consumption. In the best case for the obtained results, there was a reduction of fuel consumption by 3.7% in CNG buses. The previous results of the nanolubricants were showed very effective in fuel economy improvement owing to reduce frictional power losses directly as result smart operating and adapting according to the automotive engines requirements. That is why nanolubricants have gained tremendous attention as a promising direction for scholars and manufactures. The basic question of why we have selected this type of nano-additives (Gr) is satisfactorily responded. The 2D Gr nano-sheets have intriguing features as high thermal conductivity and outstanding mechanical properties [32]. Gr nano-sheets offer superior chemical stability and they can serve effectively in different tribological applications. Gr have lots of potentials such as anti-friction/wear, acting as solid lubricants on sliding worn interfaces, which lead to a longer lifespan for engine parts and improving engine durability [33]. In addition, Gr provides weak forces of the van der Waals and electrostatic interactions forces between the 2D layers, which help in the stability of nanolubricants [34].

The novelty in this article is the presenting of the mechanisms responsible for the tribological events (anti-friction and anti-wear) of the piston ring/cylinder liner interfaces using Gr nanolubricant compared to the traditional lube oil (5W-30). Besides, we discussed the composition and morphology of the tribo-chemistry films formed on the worn surfaces using tests of FE-SEM, EDS, 3D surface profiler, XPS, and Raman spectroscopy (Section 3.3). The engine performance was assessed by AVL dynamometer with road load simulation under New European Driving Cycle (NEDC) and provide a positive contribution to fuel economy and exhaust emissions.

2. Experimental section

2.1. Characterization of Gr nanostructures

The morphology and characterization of Gr nanostructures were identified by scanning electron microscopy (SEM), transmission electron microscopy (TEM) and X-ray diffraction (XRD). As noted in Fig. 1a consistently distributed G morphology can be observed. The high-resolution (HRTEM) images of the G is shown in Fig. 1c and d. In XRD pattern, a sharp reflection and another weak reflection in the XRD pattern of G locate at 2θ = 26.381° and at about 2θ = 54.542° which are attributed to (0 0 2) and (0 0 4) crystal planes of hexagonal graphite. Obviously, the peak at 2θ = 26.381° in XRD spectrum matches with ICSD No. 98-005-2916 [10,35]. This results obviously showed that the crystalline structure of the G was intact. Furthermore, the technical specifications of the Gr nano-sheets are listed in Table 2 (Nanjing XFNANO Materials Tech Co., Ltd). The average diameter and thickness of the Gr nanomaterials are 5–10 μm and 3–10 nm, respectively.

2.2. Formulation of Gr nanolubricant

In this study, the commercial lubricant of Castrol EDGE professional A5 (5W-30) was utilized as a reference oil. As in Fig. 2, the Gr nanolubricant samples were prepared for four concentrations (0.03, 0.2, 0.4 and 0.6 wt.%). The concentrations (0.03–0.6 wt.%) of Gr were selected to obtain a stable dispersion to avoid sedimentation in the lube oil. Furthermore, the composition of the Gr nanolubricant was maintained as similar as possible to that of the reference oil as presented in Table 3. On other hand, Gr nanolubricant comprised 2 wt.% solution (Gr + oleic acid) and 98 wt.% reference oil (5W-30). The main reason for the 2% solution is that this concentration performs a very stable mixture and there is no any separation problems. Furthermore, to avoid sedimentation and aggregation of the Gr in the lube oil with time, oleic acid (OA) was utilized as a surfactant for the dispersion of the Gr in the reference oil. The mixing of the Gr nanolubricant samples was done by a mechanical stirring device for 4 h towards a homogeneous stable suspension. Table 3 reports the composition of the Gr nanolubricant samples and kinematic viscosity for the reference oil with and without OA and Gr nano-sheets in the various concentrations under 40 °C and 100 °C temperatures. The kinematic viscosity of the formulated Gr nanolubricant was measured according to the GB/T265-1988 testing standards. The addition of the Gr nano-sheets for different concentrations causes a slight surged in the viscosity as compared with reference oil. Moreover, the slight change of the viscosity could help in confirming the effect Gr nanolubricant during boundary lubrication regime. These results are in agreement with the results obtained with lube oil (5W-30) containing 0.5 wt% MoS$_2$ nanoparticles by other researchers [36].

To monitor the stability of Gr nanolubricants, dispersion analysis was carried out by UV–visible absorption (UV) spectroscopy. Fig. 3a shows absorptivity vs. wavelength for Gr nanolubricant and lube oil (5W-30) to monitor the stability of the Gr nanolubricant sample. The

Table 3
The compositions of Gr nanolubricant samples.

| Lube oil type	Concentration (wt.%)	Reference oil (5W-30)	Additive solution	kinematic viscosity (mm^2/s)	
				40 °C	100 °C
Base Oil	0[a]	100% oil	0% Gr additives	54.06	9.42
		98% oil	2% oleic acid	54.09	9.42
Gr Nanolubricant	0.03	98% oil	2% Gr solution (0.03 Gr + 1.97 OA)	54.90	9.50
	0.2	98% oil	2% Gr solution (0.2 Gr + 1.8 OA)	55.60	9.90
	0.4	98% oil	2% Gr solution (0.4 Gr + 1.6 OA)	56.00	10.00
	0.6	98% oil	2% Gr solution (0.6 Gr + 1.4 OA)	56.34	10.20

[a] Base oil (5W-30) without Gr.
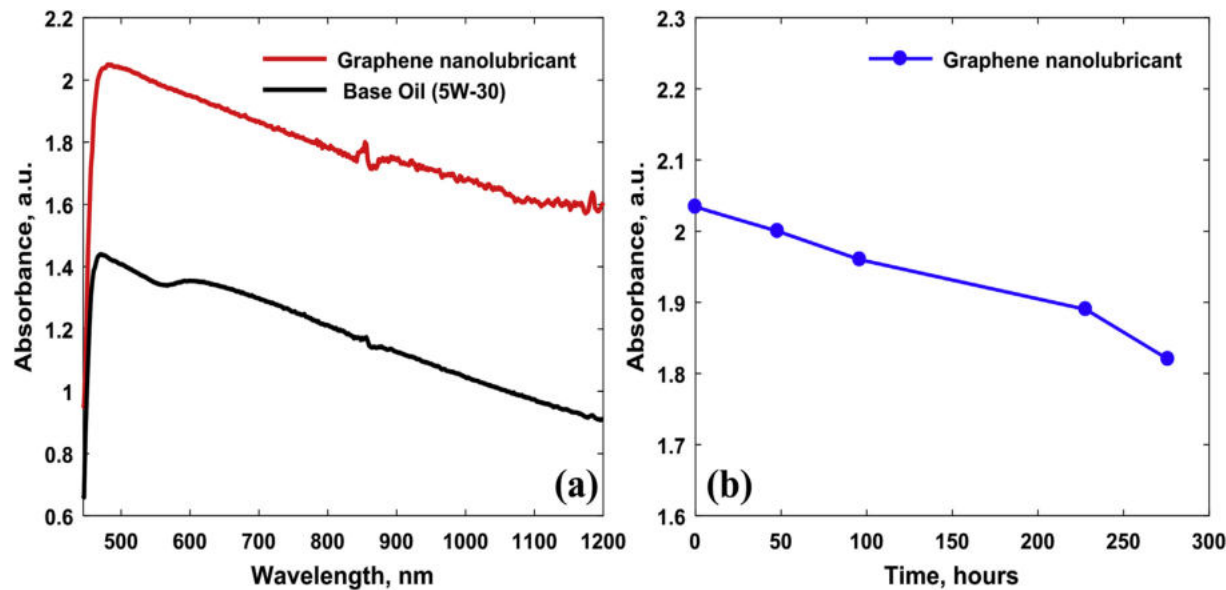
Fig. 3. UV analysis of the Gr nanolubricant samples. (a) UV analysis for both of a reference oil (5W-30) and Gr nanolubricant (0.4 wt.% G) with respect to the wavelength directly after preparation. (b) UV time history for Gr nanolubricant during 11 days.
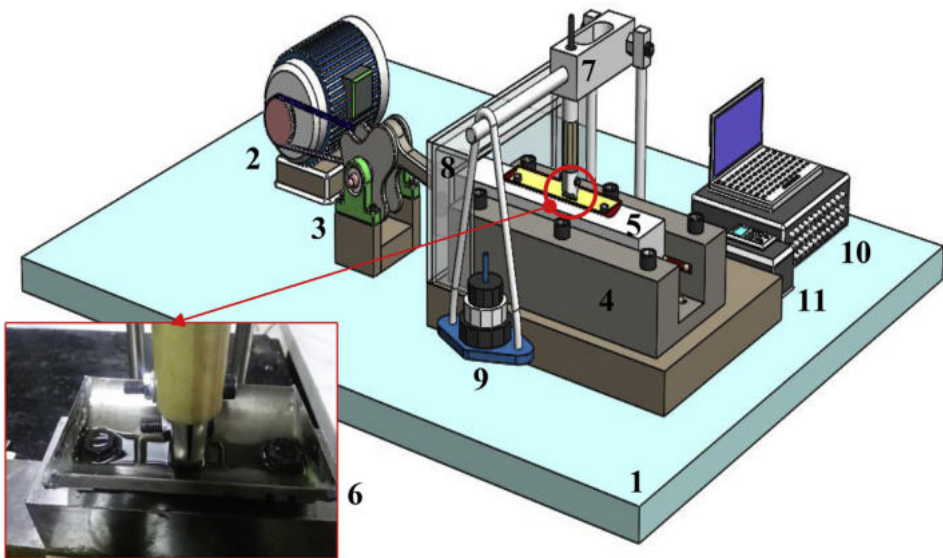

Fig. 4. Tribometer bench of the piston ring/cylinder liner interface; (1) bench base, (2) AC electrical motor, (3) crank mechanism, (4) fixed guide, (5) sliding guide, (6) ring/cylinder assembly with nanolubricant, (7) force sensor, (8) controllable temperature room, (9) weights, (10) data acquisition system and PC, (11) speed controller.
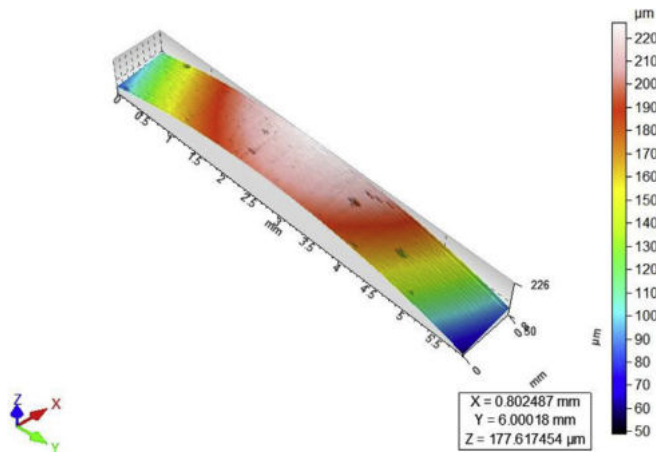

Fig. 5. The profilometric of running face for piston ring surface.

Table 4
Specifications of a HXDG16-BD-TJ gasoline engine.

| Parameter	Value	Parameter	Value
Engine specifications (HXDG16-BD-T)			
Fuel	Gasoline	No. of cylinders	4-Cylinders
Type	4-stroke	Swept volume (litters)	1.6
Cylinder bore (mm)	75	Compression ratio	10.5:1
Cylinder stroke (mm)	90.5	Max Torque @ 4000–4500 rpm (N.m)	160
Max Power @ 5600 rpm (kW)	85	Idle speed (rpm)	770 ± 50
Fuel injection system	Multi-point	Ignition system	Independent
Cooling type	Water		
Vehicle specifications used in NEDC simulation			
Gross vehicle weight (kg)	1690	Transmission system	Manual
Gear ratios	5, 3.417,1.81, 1.27, 0.975		
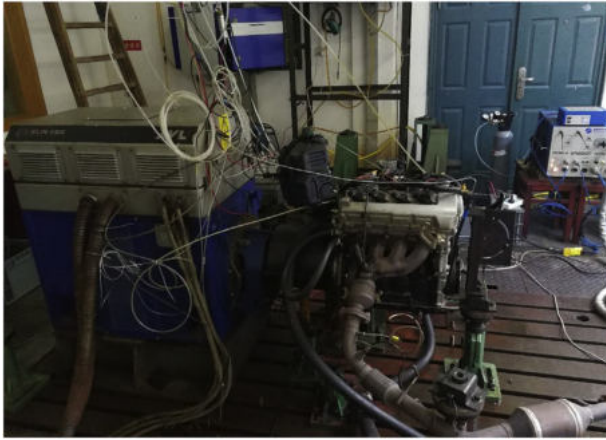
Fig. 6. AVL test bench fitted with a 1.6 litter gasoline 4-cylinder engine used in the study.
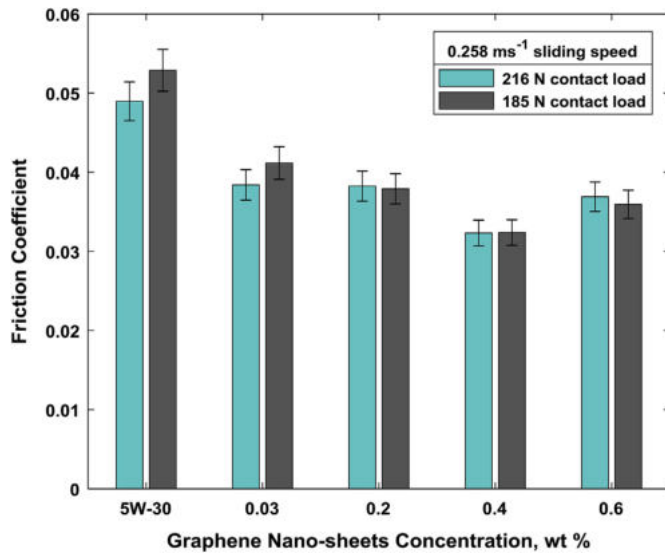

Fig. 7. The average friction coefficient between sliding contact surfaces as a function of Gr nano-sheet concentrations.

comparison between the UV spectrum peaks provided max peaks at a wavelength of (λ_{max}) of 482 and 470 nm for Gr nanolubricants and lube oil (5W-30), respectively, after preparation (at time = 0). The higher peak of absorbance level implies a better distribution of the Gr within the lube oil. The stability of the Gr nanolubricant formulated was monitored for 11 days as shown in Fig. 3b. It was evident that the Gr nanolubricant stability depends on the time, which decreased with increasing the storage time after the preparation due to sedimentation of the Gr in the reference oil. Based on the UV results, the time plays a vital role in the stability of the Gr nanolubricant. Hence, more study and discuss the influencing factors on the dispersion of the nano-additives in lubricant oils will be required for overcoming the aggregation problem during a longer time. The aggregation of nano-additives occurs whenever the Brownian motion and Van der Waals attractive forces of the nano-additives were greater than the repulsive forces based on Derjaguin, Landau, Verwey and Overbeek developed the (DLVO) theory [37].

2.3. Worn surface analysis

The Crystalline structure of the Gr was determined by X-ray diffraction (XRD) test using CuKα radiation at 30 kV and 40 mA at a scanning speed of $0.01°s^{-1}$. Then, the XRD data were analyzed with the

assistance of MDI Jade 6 program. To evaluate the morphologies of the worn surfaces of the ring and the liner samples, the field-emission scanning electron microscopy (FE-SEM, ZEISS ULTRA PLUS) was used. The deposition of the Gr tribofilm on the worn surfaces was examined via energy dispersive spectroscopy (EDS, Inca X-Act). X-Ray photo-electron spectrometry (XPS, Thermo model ESCALAB250) was used to assess the chemical structure of a tribofilm. Raman spectroscopy was utilized to study the chemical bonding in the tribofilms formed on the rubbing surfaces. Whilst, The surface roughness of the frictional specimens (piston ring and liner) was measured using a Nanovea ST400 3D Profilometer (non-contact profilometer).

2.4. Tribometer test rig description

During the current study, based on ASTMG181, tribometer bench of ring/liner assembly are designed for simulating the sliding reciprocating motion of the piston ring/cylinder liner contact as shown in Fig. 4. The details of the reciprocating tribometer and their characteristics were reported in our previous publications [11]. The specimens of a compression ring and liner used in the tribological tests were fragments of an actual petrol engine for better comparison and analysis based on the materials same as those found in an internal combustion engine. The average hardness of the liner surface was 413 VH (Vickers hardness), whilst the hardness of the ring was 320 VH. In terms of friction and wear characterization, for one test results, the speed and load were fixed and the signals were recorded in which the same test was repeated three times and the average results among them were considered.

2.5. Tribological testing procedures

The tribological behavior of the proposed samples was investigated using the piston ring/liner reciprocating tribometer. The tribological tests were performed at the room temperature, different sliding speeds from 0.154 to 0.6 m/s and contact loads ranged from 90 to 368 N, which corresponds to pressures ranging from 1.95 to 7.9 MPa, respectively. This pressure describes the highest nominal radial pressure occurred between the ring and liner during actual engine operation (Hydra engine) after the combustion under 50% of maximum engine load [38]. To elucidate the lubrication regime, Lambda ratio and the oil film thickness were determined using Equations (1) and (2), respectively, suggested by Hamrock and Dowson [39].

$$\frac{h_{min}}{R} = 3.63 \left(\frac{U\,\gamma}{E\,R} \right)^{0.68} (\alpha\,R)^{0.49} \left(\frac{W}{E\,R^2} \right)^{-0.073} (1 - e^{-0.68\,k}) \tag{1}$$

$$\lambda = \frac{h_{min}}{\sigma_{rms}} = \frac{h_{min}}{\sum R_q} = \frac{h_{min}}{\sqrt{R_{q1}^2 + R_{q2}^2}} \tag{2}$$

where h_{min} is the minimum oil film thickness, R is radius of curvature of the ring, U is the entraining surface velocity, γ is the dynamic viscosity of the lube oil at atmospheric pressure, α is the viscosity pressure coefficient, W is the contact load, E is Young's modulus, σ_{rms} is the root mean square roughness of the ring and liner surfaces, R_{q1} is the surface roughness of the ring and R_{q2} is the surface roughness of the liner. Based on tribological test conditions, surface roughness measurements and material parameters, the calculated lambda ratio (λ) was not exceeding 0.87, which confirm that the contact conditions were within the boundary lubrication regime. The boundary lubrication regime happens very often when an element starts relative motion with very low speed and high load. In automotive engines, the boundary lubrication regime is found in the cold starting/stopping conditions of the engine. For example, journal bearings undergo in the boundary lubrication regime during starting/stopping. Additionally, the boundary lubrication happens permanently during engine running in the piston ring assembly at the bottom and top dead centers of the
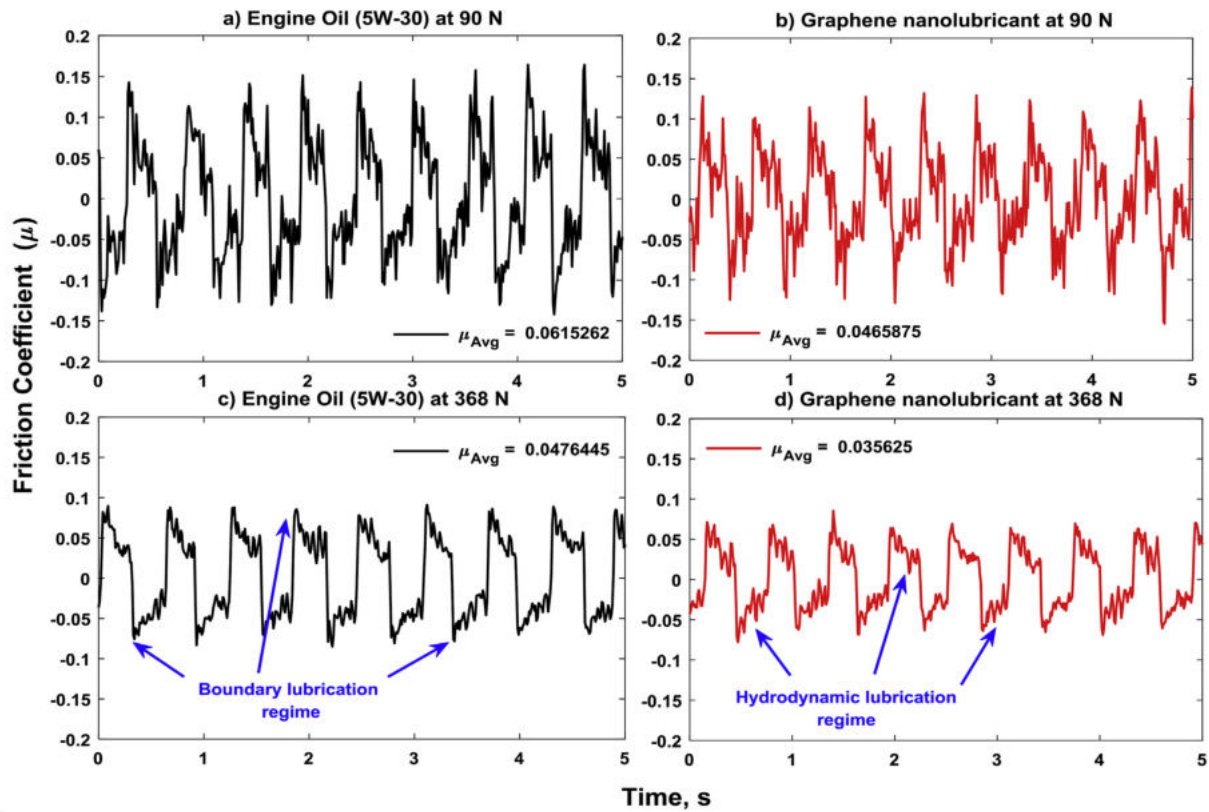
Fig. 8. Time history ~~part from~~ the friction coefficient signal of piston ring assembly at the minimum and maximum load; (a and b) the friction signal at 90 N (1.95 MPa) for both lube oil samples, (c, and d) the friction signal at 368 N (7.9 MPa) for both lube oil samples.
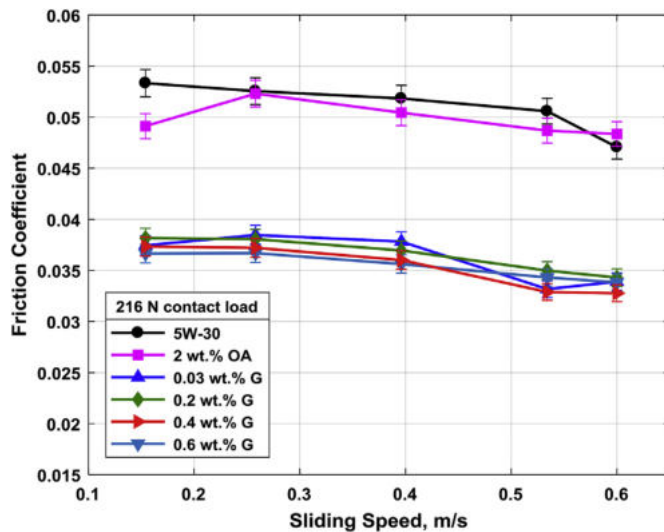

Fig. 9. The average friction coefficient between worn surfaces lubricated by reference oil (5W-30) and Gr nanolubricant with respect to the sliding speed.

Fig. 10. The average friction coefficient between worn surfaces lubricated by reference oil (5W-30) and Gr nanolubricant with respect to the contact load.

stroke and the valve train system.

In this set-up, the ring and liner were segmented into several equal specimens in dimensions for using as frictional specimens. To obtain reliable data from tribological tests, the ring and liner specimens were allocated for each test point at studying the effect of the load and speed on the friction and wear tests. Besides, one segment of the ring and liner were allocated for both reference oil (5W-30) and Gr nanolubricant when studying the effect of sliding distance on the wear and monitor the wear during different sliding distances. Before starting experiments, the frictional specimens were ultrasonically cleaned in acetone and
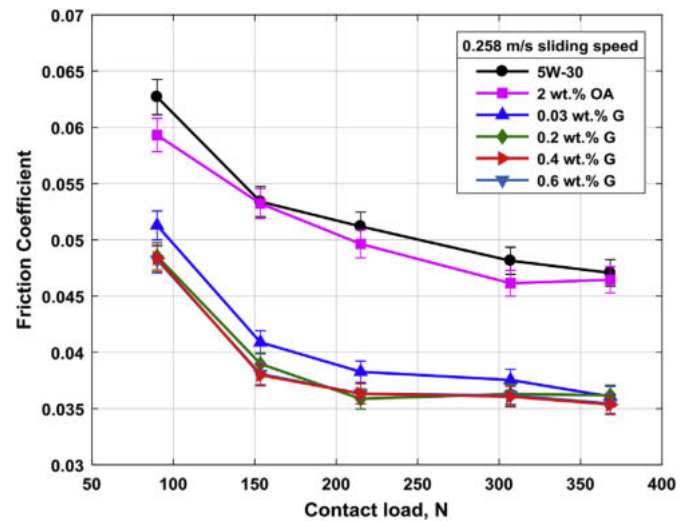
dried. It is worth mentioning that the wear rate of the ring was determined based on the aforementioned equation [9]:

$$\text{Wear rate of the ring} = \frac{V}{W \cdot S} \tag{3}$$

Where V is the worn volume (mm^3), W is the normal contact load (N) and S is the sliding distance (m).

Fig. 5 illustrates the profilometric of the piston ring surface which is used in wear volume measurements. In the wear rate observation, before each trial, the ring-liner surfaces were washed with acetone to remove the remaining contaminants from the previous test. Every
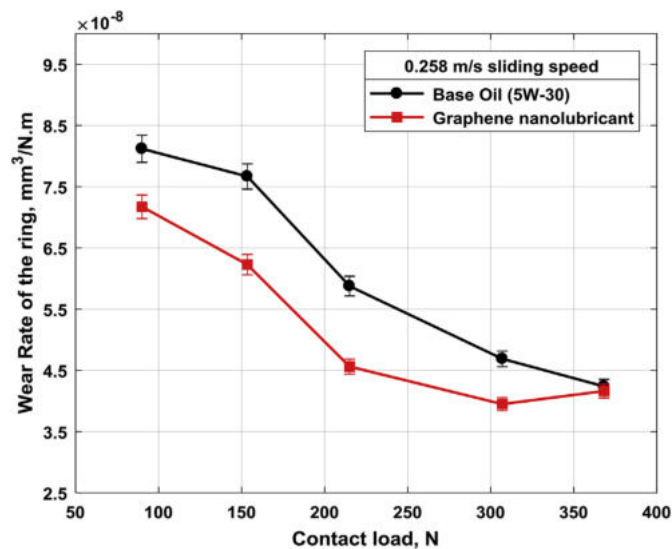
Fig. 11. Wear rate of the ring for the Gr nanolubricant against reference oil (5W-30) with respect to different contact loads and 0.258 m/s sliding speed.
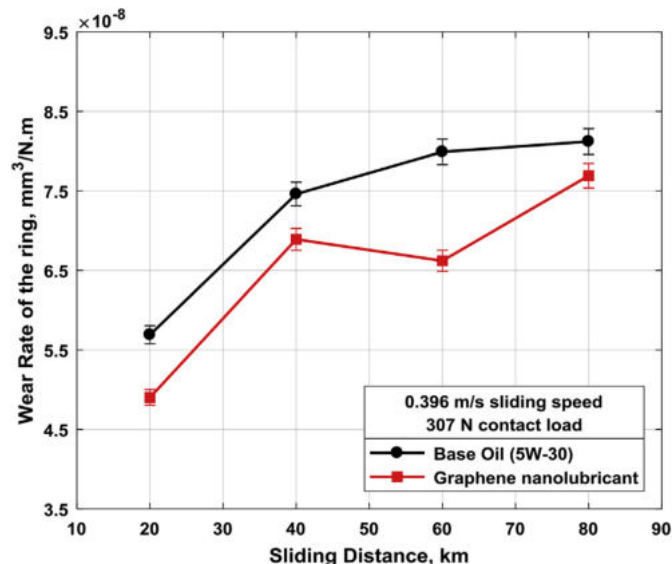

Fig. 12. Wear rate of the ring for the Gr nanolubricant against reference oil (5W-30) with respect to different sliding distances.

friction experiment was conducted for the duration of 30 min. The wear and friction tests were conducted at least three times under the same experimented conditions in an attempt to replicate the tests to obtain reliable data, after which the average results were taken.

2.6. Engine testing

To link tribological tests in the laboratory with actual engine performance, the engine performance was evaluated utilizing AVL dynamometer under various speeds and loads of the engine and New European Driving Cycle (NEDC).

2.6.1. Engine specifications

The engine performance experimentations were executed on a gasoline engine. The engine specifications are given in Table 4. The engine was attached to AVL dynamometer (Fig. 6) to measure the engine performance under the lubrication using reference oil (5W-30) without Gr and then with the Gr nanolubricant. The AVL dynamic fuel meter balance was utilized for measuring the fuel consumption. Additionally,
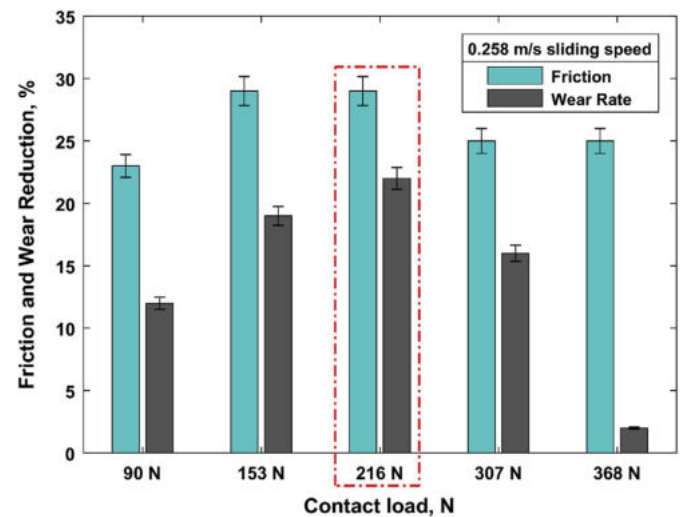

Fig. 13. The reduction in the friction and wear trends with respect to different contact loads and 0.258 m/s sliding speed during the lubrication by Gr nanolubricant.

the AVL dynamic fuel meter balance was connected with the AVL PUMA system in order to measure an actual fuel consumption based on actual operating parameters e.g. temperature, pressure, and load such that corrected fuel consumption signal is obtained in the displayed test results. Besides, the engine parameters were controlled as well as monitored and the results displayed by a PC interface (AVL PUMA software) that was directly connected to the engine ECU.

2.6.2. Engine testing conditions

The laboratory experiments in this investigation were performed at various engine speeds ranging from 1000 to 4000 rpm, with an interval of 250 rpm under throttle valve positions of 50 and 75%. The recorded results included the engine brake power, torque, total frictional power, fuel and gasses emissions (carbon dioxide (CO_2), carbon monoxide (CO), nitrogen oxides (NO_x), and hydrocarbons (HC)). SEMTECH-G exhaust gas analyzer is used to measure the exhaust emissions. The test begins only after the engine reached a thermal steady-state. The engine was regarded as warm meanwhile the lubricant oil and coolant were kept at range from 70 to 90 °C and 85 °C, respectively. To measure the frictional power losses by the hot motoring test, the engine was operated various speeds with the throttle wide open since the pumping losses were eliminated (nearby to zero) [1]. During the hot motoring test, the lube oil and water temperatures were maintained at 70–90 °C and 85 °C via heated before starting the test, respectively, as in the fired engine. The measurements were repeated three times under the same conditions in an attempt to replicate experimental results and the average values were considered as final results, which ensure the reliability of the outcomes to judge the engine performance.

Additionally, the engine was experimented under NEDC to investigate the effect of the Gr nanolubricants on the fuel in real working conditions. The NEDC contains four urban driving stages (ECE) during first 780 s time characterized by low engine load and low vehicle speed followed by motorway driving stage (EUDC) for 400 s (driving under high-speed). Additionally, NEDC consists of the deceleration and acceleration (transient phases), idle phase and the steady state (constant velocity). Every NEDC test was started at a cold-starting of the engine (18–20 °C) and ended in the range between 70 and 90 °C for the lube oils used in tests. Besides, every NEDC test was repeated three times with similar test conditions to obtain reliable results.
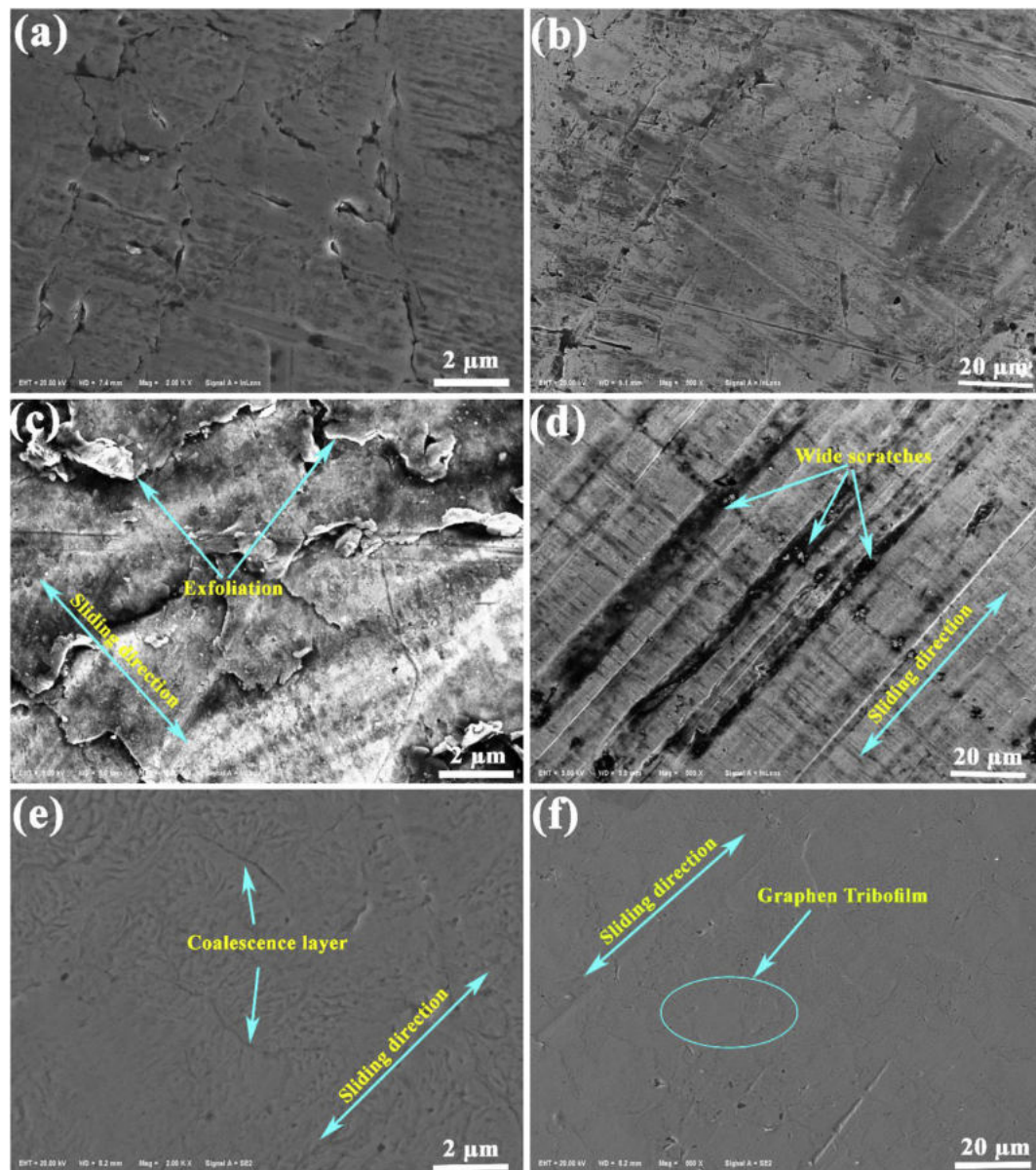
Fig. 14. FE-SEM images of the friction surface of the piston ring; (a) Piston ring surface before sliding, (c) Use of a reference oil (5W-30), (e) Gr nanolubricant, (b, d and f are magnified images of a, c, and e, respectively).

3. Results and discussion

3.1. Effect of Gr concentration on the friction

To determine the optimum concentration of the Gr nano-sheets in the reference oil (5W-30), the coefficient of friction (COF) was monitored under different concentrations of Gr nano-sheets (0.03, 0.2, 0.4 and 0.6 wt.%). Fig. 7 presents the COF trends for these concentrations under 185 N and 216 N contact load (correspond to 4.01 MPa and 4.69 MPa contact pressure) and an average sliding speed of 0.258 m/s. Although all concentrations of Gr nanolubricant reduced the COF comparing to the 5W-30 oil, the concentration of 0.4 wt.% Gr nano-sheets obtains the minimum friction trend (35% reduction) among the other samples. This can be explained by the contact area between the rubbing surfaces is related to the scale of surface asperities owing to the boundary lubrication. These conditions may benefit from the nanoscale dimension of the Gr filling the valleys between asperities by Gr nano-sheets, which helps to reduce the boundary friction coefficient. However, after a certain concentration, the contact area was saturated by nano-additives and any more Gr nano-sheets will not be helpful. Besides, the agglomeration of the Gr is probable to occur in the lubricant using higher concentrations, which can be larger than the oil film thickness in the contact area causing friction increase. The optimum concentration is 0.4 wt.% where the contact area is saturated with Gr nano-sheets and the surface contact areas cannot contain more solid additives. Hence, the concentration of 0.4 wt.% Gr nano-sheets was used for further tribological investigations in the current study. From Fig. 7, it can be seen that the high load (216 N) exhibited a reduction in coefficient of friction, especially at reference oil and 0.03 wt.% Gr, as compared with low load (185 N). This might be due to the increase of the contact pressure over the asperities tips and Gr (mechanically unstable), which helps to form tribofilms on the rubbing surfaces to separate the asperities.

3.2. Tribological performance of Gr nanolubricant

3.2.1. Anti-friction behavior

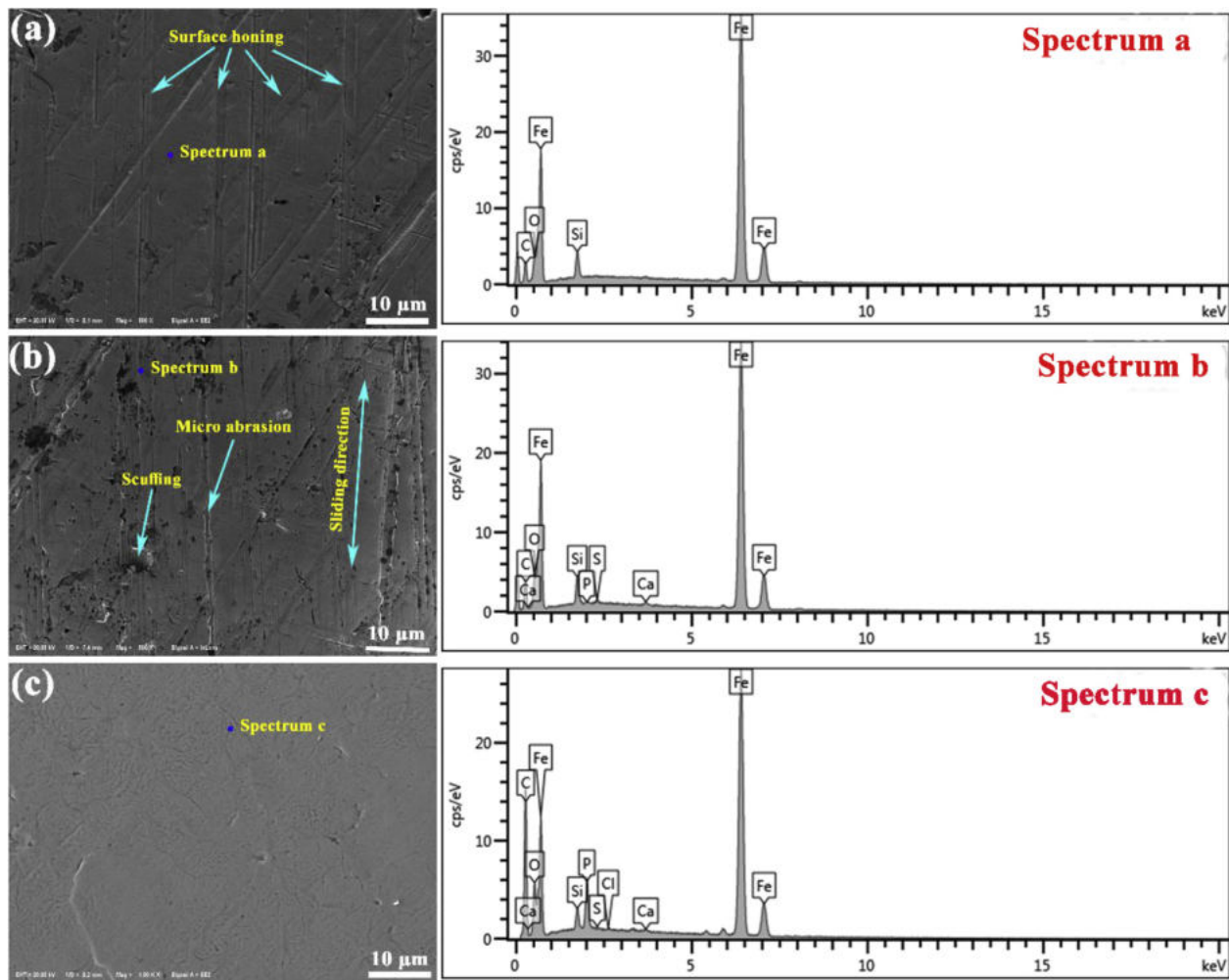The output friction coefficient signal is presented in Fig. 8 for both a

Fig. 15. EDS patterns of the piston ring worn surface; (a) Piston ring surface before sliding; (b) Use of a reference oil, (c) Gr nanolubricant with a concentration of 0.4 wt.%.

Table 5
Elements content of the piston ring worn surface based on EDS results.

Elements	Spectrum a (Before sliding)		Spectrum b (5W-30)		Spectrum c (Gr nanolubricant)	
	Weight %	Atomic %	Weight %	Atomic %	Weight %	Atomic %
C	12.57	37.29	15.95	43.00	20.05	50.32
O	3.38	7.53	4.66	9.43	3.34	6.30
Si	2.46	3.12	2.32	2.68	1.21	1.30
P	–	–	0.16	0.17	3.01	2.93
S	–	–	0.18	0.18	0.05	0.05
Cl	–	–	–	–	0.09	0.07
Ca	–	–	0.26	0.21	0.19	0.14
Fe	81.59	52.05	76.46	44.32	72.06	38.89
Total	100	100	100	100	100	100

reference oil sample and Gr nanolubricant with a concentration of 0.4 wt.% at 90 N and 368 N contact load (1.95 MPa and 7.9 MPa contact pressure). The friction behavior corresponding to Gr nanolubricant showed lower trend compared with the oil without nano-additives. The maximum friction was found at TDC and BTC due to the boundary lubrication regime (Fig. 8c) in these locations, while, the friction was minimum at mid-stroke owing to in the hydrodynamic regime (Fig. 8d) [11]. Looking at Fig. 9, the influence of the sliding speeds on the friction coefficient trend for a 216 N normal load (4.69 MPa) is provided for the previously mentioned lubrication samples in Section 2.2 (5W-

30, 2 wt.% OA, 0.03 wt.% Gr, 0.2 wt.% Gr, 0.4 wt.% Gr, and 0.6 wt.% Gr). The fabricated experimentations showed that the friction trend declined with the growth of sliding speed for all of the tested samples. The separation distance of the sliding surfaces grows with the increase of the sliding speed, what makes the contact area of the worn surfaces decreased leading to a decline in the friction coefficient. Moreover, for higher sliding speed, there is less time for the individual asperity contacts and, consequently, less time for asperities to deform [40]. Based on the obtained results from Fig. 9, it was evident that all concentrations of Gr nanolubricant presented similar values in the reduction of the friction coefficient in the ranges 29–35% during various sliding speeds, as compared with a reference oil.

Furthermore, there is a clear trend of decreasing in the friction coefficient in Fig. 10 with respect to the contact load growth for both reference oil and Gr nanolubricant. The reason for this decline may be due to the severity of the contact pressure over the asperities under high contact loads. Some of the asperities may fracture or crush, leading to smoother surface and reduction in the boundary friction coefficient. On the other hand, this might be due to the elastohydrodynamic lubrication, which the lubricant pressure is high enough to deform both liner and piston ring surfaces, creating a gap filled by the lubricant leading to reduced friction. It also could be that at high load the piston ring area in contact with the liner increases due to deformation, changing the contact pressure to less significant magnitudes, hence, reducing the friction coefficient. Whereas, Gr nanolubricant was enhanced the anti-friction property by 23–29% at a constant sliding rate and different
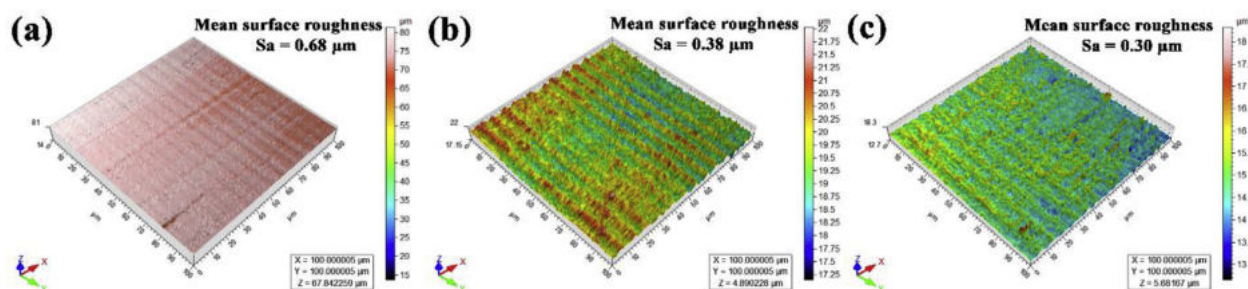
Fig. 16. 3D surface profiler images of the piston ring; (a) Piston ring worn surface before sliding, (b) Use of a reference oil, (c) Gr nanolubricant with a concentration of 0.4 wt.%.

contact loads owing to tribofilm formation on the worn sliding surfaces. Likely due to a synergy between Gr nanolubricant, ZDDP in engine oil and worn surfaces as shown in Fig. 17. Interestingly, the change in friction coefficient values was not significant at higher loads in Gr nanolubricants. Although, at reference oil without Gr, a noteworthy change in friction coefficient was seen suggesting a slower tribofilm formation during high loads.

3.2.2. Anti-wear behavior

In order to evaluate anti-wear properties, we studied the effect of contact loads and sliding distance on the wear rate of the piston ring for both of the reference oil and Gr nanolubricant with a concentration of 0.4 wt.% as highlighted in Figs. 11 and 12. Fig. 11 elucidated that the wear rate is decreased for both of the lubricants with and without Gr nano-sheets with increasing the contact loads. The lower wear rate under higher contact load can be explained as the wear debris are sintered back into the worn surface of the ring. This implies that the wear debris was contributed in the self-lubricating layers formed on the worn surfaces during lubrication by Gr nanolubricant. Furthermore, the rubbing surfaces temperature becomes greater with increasing the load, which lead to thermal activation of the wear debris with Gr nano-additives and thus helps the strong cohesion of the self-lubricating layers with worn surfaces. The results exhibited a decrease in the wear rate for the use of Gr nanolubricant by 22% as compared with base oil without Gr nano-sheets when the contact load and average sliding speed were 215 N (4.66 MPa) and 0.258 m/s, respectively. The major reason for the decrease in the wear rate is the formation of the tribo-layers on the worn surfaces, acting as a self-coating, as shown in Fig. 17e.

The wear results in Fig. 12 presents the wear rates of the ring versus the various sliding distance for both of the reference oil and Gr nanolubricant under 307 N contact load (6.66 MPa) and 0.396 m/s sliding speed. The results explained that the wear rates of the ring specimens for both lube oils were increased with increasing of the sliding distance owing to the frictional surface is no longer able to continue the oxide layer and wear mechanism changed from tribo-oxidation to adhesion. It is obviously seen that Gr nanolubricant can significantly reduce the wear rate of the ring, in comparison with reference oil. Hence, the major mechanism of Gr nanolubricant was self-replenishment of the self-lubricating layers, which help in the self-healing of the worn surfaces as shown in Fig. 17e. For a sliding distance between 40-60 km, the self-lubricating layers had a great anti-wear resistance. It is noteworthy that the Gr nanolubricant at 60 km sliding distance was more effective in improving the self-lubricating layers, as compared with 40 km and 80 km sliding distance. This might be related to the embeddability of the wear debris into the ring sample that often called cold welding or smearing.

In order to have a better picture of the Gr nanolubricant effect on the tribological behavior of the contact surfaces under the boundary lubrication regime, the reduction in the friction and wear for base oil and Gr nanolubricants were plotted at a constant average sliding speed of 0.258 m/s and with respect to different contact loads (see Fig. 13).

The maximum enhancement of the anti-wear and anti-friction properties were achieved under a contact load of 216 N (4.69 MPa) being 22% and 29%, respectively. Mainly, the reason for the decline in the friction coefficient and wear rate is the Gr tribofilm formation on worn surfaces, acting as an ultra-thin surface coating that decreases the shear effect. Otherwise, the wear rate increased with the contact load over 216 N, this phenomenon may be due to the slower build-up of a tribofilm under very high loads. Whilst, it can be seen that Gr nanolubricants play an important role in the friction behavior under high loads.

3.3. Elucidation of the anti-friction/wear mechanisms

This section provides an explanation of the mechanisms and tribochemistry to understand the tribological behavior performed of the Gr nanolubricant with a concentration of 0.4 wt.% on the worn surfaces that is responsible for the enhancement of the anti-friction and anti-wear behavior. Morphologies tests were after a 60 km sliding distance under 216 N contact load (4.69 MPa) and 0.258 m/s average sliding speed. Fig. 14 compares the FE-SEM results of the ring surface before the beginning of the test, with 5W–30 engine oil, and with Gr nanolubricant. The major lineaments of the topography of the frictional surface are highlighted including the sliding direction. As a general observation: some exfoliations and adhesive phenomena occurred as shown in Fig. 14c and d, as well as wide scratches appeared in the same direction as the sliding due to micro-abrasive wear due to a tribofilm losing on the worn surfaces and becoming not smooth during sliding.

This would account for the increase in the measured friction coefficient and wear rate at use lube oil alone as shown in Figs. 9–11. Hence, engine oil eventually was unable to separate the asperities contacts effectively, and grooves appeared on the worn surface Fig. 14d. The resultant boundary tribofilm inhibited the plastic deformation of asperities to some extent, but the valleys of the plowing grooves and the surface micro-cracks became increasingly intensive on the worn ring surface as shown in Fig. 14d. This was associated with the gradual depletion of tribofilm form traditional additives of the engine oil. While, the lubrication using Gr nanolubricant prevents adhesive wear and exfoliations and micro-abrasive on the worn surfaces. It is clearly observed from Fig. 14e and f that there is a Gr tribofilm formed on the ring worn surface covering the wide scratches leading to smoother surface and less abrasive wear. Moreover, the formation of the Gr tribofilm helped in the healing and coalescing of the cracks and scratches of the piston ring surface. The synergetic effects of Gr nanolubricant and lube oil resulted in excellent anti-friction and anti-wear properties (Figs. 9 and 11).

The EDS patters of the piston ring worn surface are provided in Fig. 15 for the ring surface before sliding against the engine oil and Gr nanolubricant. Furthermore, Table 5 summarized and compared the distribution of elements found in each case. Generally, greater C and P was reported on the ring lubricated by Gr nanolubricants than ring lubricated by 5W–30 oil. This reveals that the boundary tribofilm formed on the ring was thicker due to the addition of the Gr nano-sheets
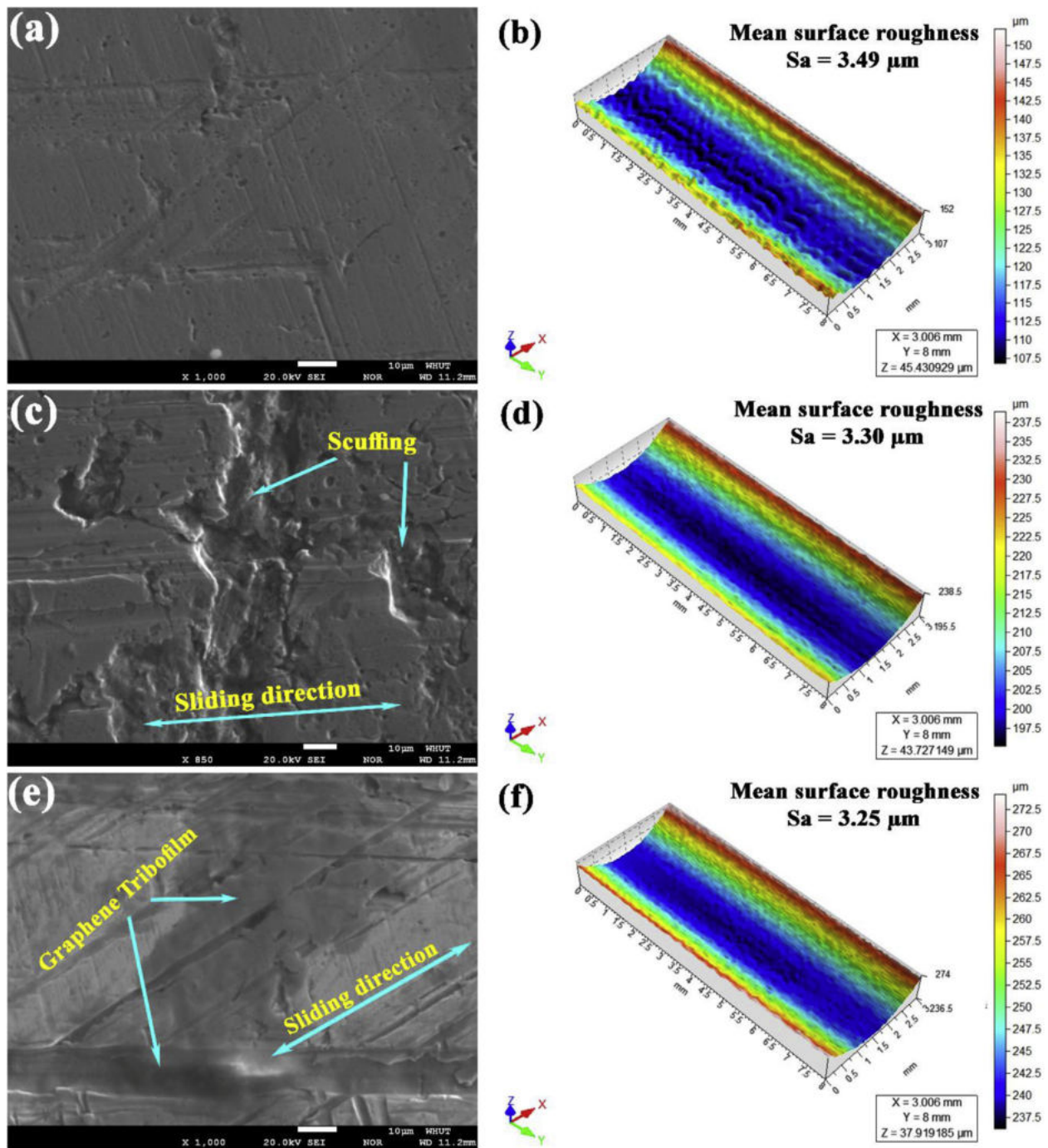
Fig. 17. SEM and 3D surface roughness of the cylinder liner; (a, b) Liner surface before sliding; (c, d) Use of a reference oil, (e, f) Gr nanolubricant with a concentration of 0.4 wt.%.

into the lube oil. For a complete observation of the tribological performance, 3D surface roughness profile of the ring are presented in Fig. 16. The results are shown that the mean surface roughness values of the piston ring were 0.68 μm, 0.38 μm and 0.30 μm for before sliding, using commercial lubricant, using Gr nanolubricant, respectively.

Furthermore, the opposing cylinder liner surface showed common wear characteristics in Fig. 17c, including scuffing, cracks, and big pits due to a material being removed by adhesive wear, which dominated the liner worn surface. The liner worn surface was relatively smooth and featureless showing normal polishing wear using Gr nanolubricant (Fig. 17e). Although some pits and spalling occurred in some local areas as well as micro-cracks. The surface roughness parameters of the ring

and liner samples before and after each test was investigated, as shown in Table 6. Interestingly, rougher surfaces were observed for both lube oil without Gr nano-sheets and Gr nanolubricant after sliding test. Accordingly, this confirms that the reduction in friction coefficient during various speeds and loads is further controlled by the tribofilm formed on the worn surfaces rather than the surface roughness.

Fig. 18 provides the EDS patterns and microstructure of the elemental composition in the line-scanning region of the liner for both engine oil and Gr nanolubricant. The main elements of the boundary tribofilm and their distribution on the liner worn surface are comparatively presented in Fig. 18c and d. Clear signals of C from lube oil and Gr, P, Ca, S, and O elements from lube oil could be found as well as

Table 6

3D surface parameters of the piston ring and cylinder liner samples before and after sliding for engine oil and Gr nanolubricant.

Parameters	Unit	Piston Ring			Cylinder Liner		
		Before sliding	5W-30	Gr nanolubricant	Before sliding	5W-30	Gr nanolubricant
Sq	(μm)	**0.964696**	**0.484172**	**0.396634**	**4.504897**	**4.159451**	**4.146241**
Ssk	–	−8.762572	−8.762572	0.157852	1.350694	1.438834	1.461295
Sku	–	400.850465	400.850465	2.990691	4.148173	4.008532	4.145292
Sp	(μm)	4.011847	4.011847	2.224364	18.141701	17.514055	19.485455
Sv	(μm)	50.128190	50.128190	1.766257	12.083703	10.008741	9.223270
Sz	(μm)	54.140037	54.140037	3.990621	30.225404	27.522796	28.708724
Sa	(μm)	**0.683249**	**0.387225**	**0.307965**	**3.498965**	**3.302276**	**3.250686**
Smean	(μm)	0.002811	0.002811	0.000216	0.078338	0.072600	0.075162
Sdar	(μm²)	21002.117109	21002.117109	13060.490841	24.064436	24.057192	24.055679
Spar	(μm²)	10000.000950	10000.000950	10000.000950	24.047999	24.047999	24.047999
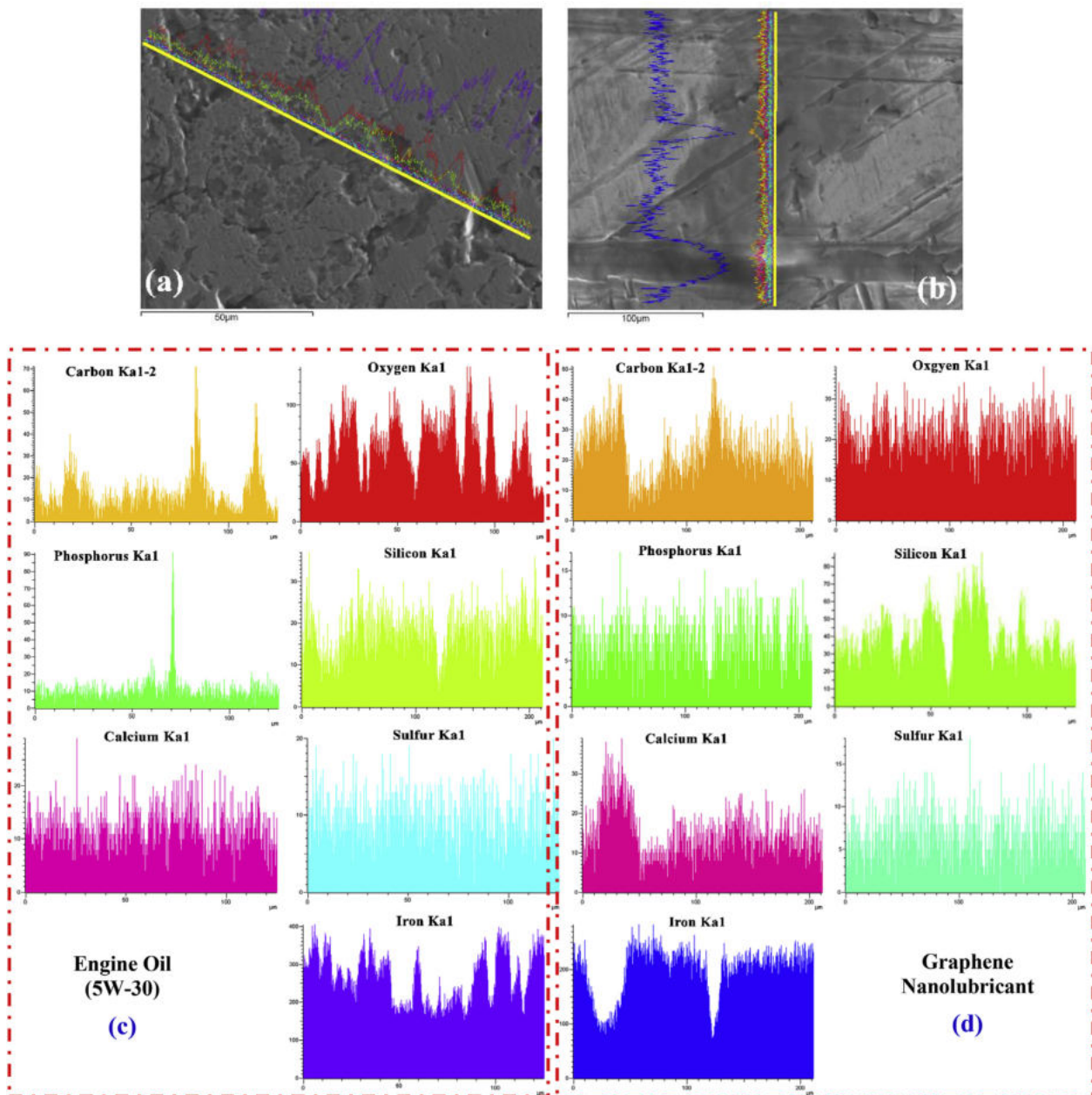
Fig. 18. Microstructure of top surface of the liner lubricated by engine oil (a), lubricated by Gr nanolubricants (b), distribution of tribofilm main elements in the line-scanning region lubricated by reference oil (c) and Gr nanolubricants (d).
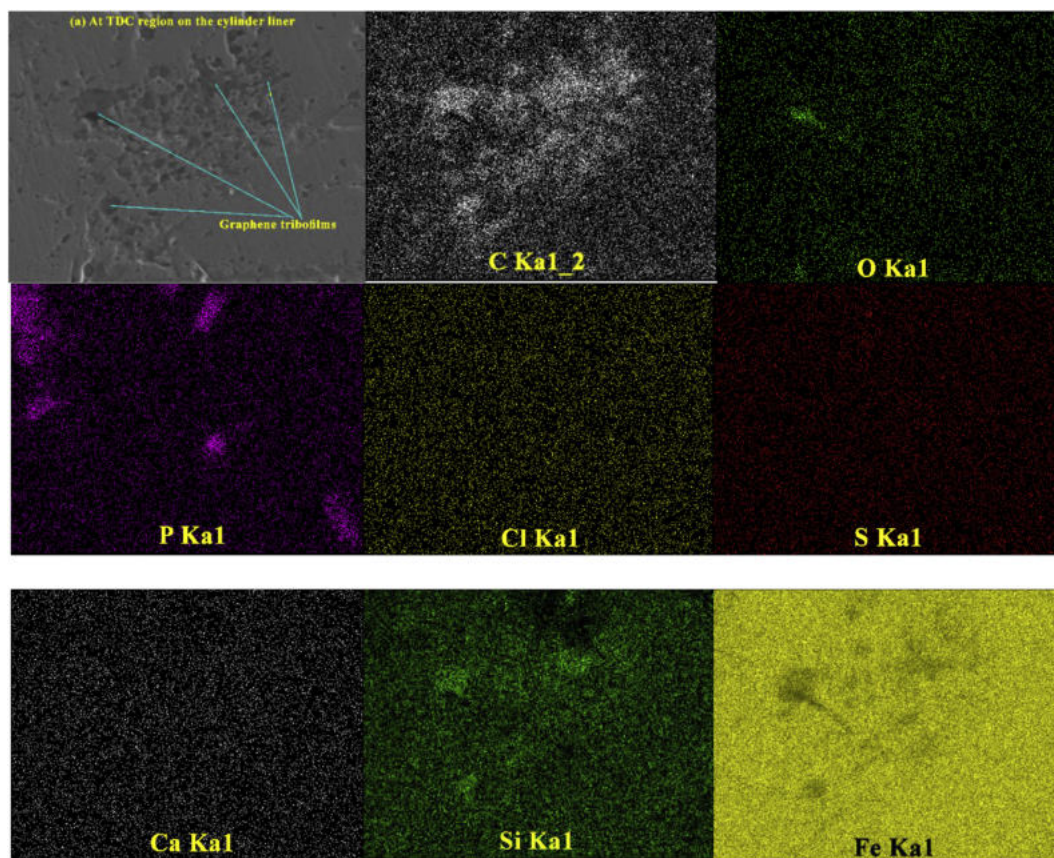
Fig. 19. Elemental distribution maps of boundary tribofilm elements at TDC region on the cylinder liner lubricated by Gr nanolubricant.

Si and Fe from the substrate worn surface of the liner. Moreover, a fraction of Ca and P was also present in the tribofilm, originating from the detergent in the oil formulation in Fig. 18d, as compared lubricant without Gr. Interestingly, the C signal was more than its level in the case of Gr nanolubricant comparing with the engine oil without Gr additives. It is apparent from Fig. 18a that the liner surface appears rough and have pits and scavenging unlike the liner surface in the Gr nanolubricant that looks smoother despite the wide grooves, but there is a tribofilm formed by Gr nano-additives that reduces the grooves depth. For example, the filling of the grooves by the Gr tribofilm confirmed by the elements distribution comparison of the oil with (Fig. 18d) and without Gr nano-additives (Fig. 18c). Another example is the P signal in which the presence of the P element in the case of oil without nano-additives was simple on the liner worn surface and it is well known that the source of the P content comes from the Zinc dialkyl-dithiophosphate (ZDDP), which suggests a slower tribofilm formation from ZDDP. In other words, the lack P on the worn surface of the liner indicates the interaction weakness of the engine oil and the liner surface in the process of tribofilm formation. While, in the case of Gr nano-additives, the P content increased that confirms the tribochemical reaction between the Gr nano-sheets, engine oil and liner worn surface helping to speed up the tribofilm formation.

Furthermore, looking at the iron patterns in Fig. 18c, the engine oil without nano-G additives provided regular distribution of the Fe content on the worn surface of the liner which gives evidence of the ineffectiveness of the traditional oil additives. However, it is further noted that the carbon content from the nano-G additives compensated the deficiency of the iron content in the wide grooves and formed a tribofilm inside the grooves and all over the liner worn surface (Fig. 18d). In G tribofilm, some wear debris of the iron formed to fill some of the wide grooves as shown in the iron pattern in Fig. 18d resulting in very smooth surfaces. At some locations, there were some black boundary

tribofilm from Gr on the worn liner surface. Furthermore, there were different acting mechanisms occurring if amorphous carbon was involved between the moving contacts [41]. A competition between ZDDP-derived tribofilm and transferring carbon has been hypothesized while carbon-catalyzed, which increases rate tribofilm formation with Gr nano-additives was reported to be responsible anti-wear properties. In summary, all the worn surfaces lubricated by Gr nanolubricant in showed typical polishing wear.

Fig. 19 present EDS elemental maps of the liner worn surface at TDC zone. Elemental mapping hints that the matrix of the boundary tribofilm is rich in C, O, P, S, Cl and Ca, likely a mixture of Fe and Si. Gr-rich tribofilms have been detected on the worn surfaces on both the ring and liner worn surfaces tested in the lubricants containing Gr nano-sheets. The worn surface lubricated by the Gr-containing oil seems to be largely covered by a layer of white color deposit as shown in Fig. 19. The high load and associated frictional heating in the boundary lubrication regime are considered to facilitate the formation of such a Gr-rich tribofilm on the worn surface. There was less oxygen in the area covered by the Gr-rich tribofilm, which indicates insignificant oxidation of the G. Although the sulfur (S) content in the tribofilm appears to be minimum.

To further elucidate, XPS test was conducted out to monitor the chemical structure and valence states of the different elements in the Gr tribofilm formed on the worn surfaces for anti-friction and anti-wear during the friction process. Fig. 20a–c display the XPS surface survey scan spectrum on the boundary tribofilm formed from engine oil alone and Gr nanolubricant compared with liner sample before friction test. The C 1s peak at 284.19 eV illustrated that C was deposited on the frictional surface of the liner (Fig. 20c), which is compatible with EDS mapping as shown in Fig. 19. Notably, the appearance of S inside a tribofilm was confirmed by the XPS spectrum, which showed a binding energy of S 2p as shown in Fig. 20b and c. These results show that the
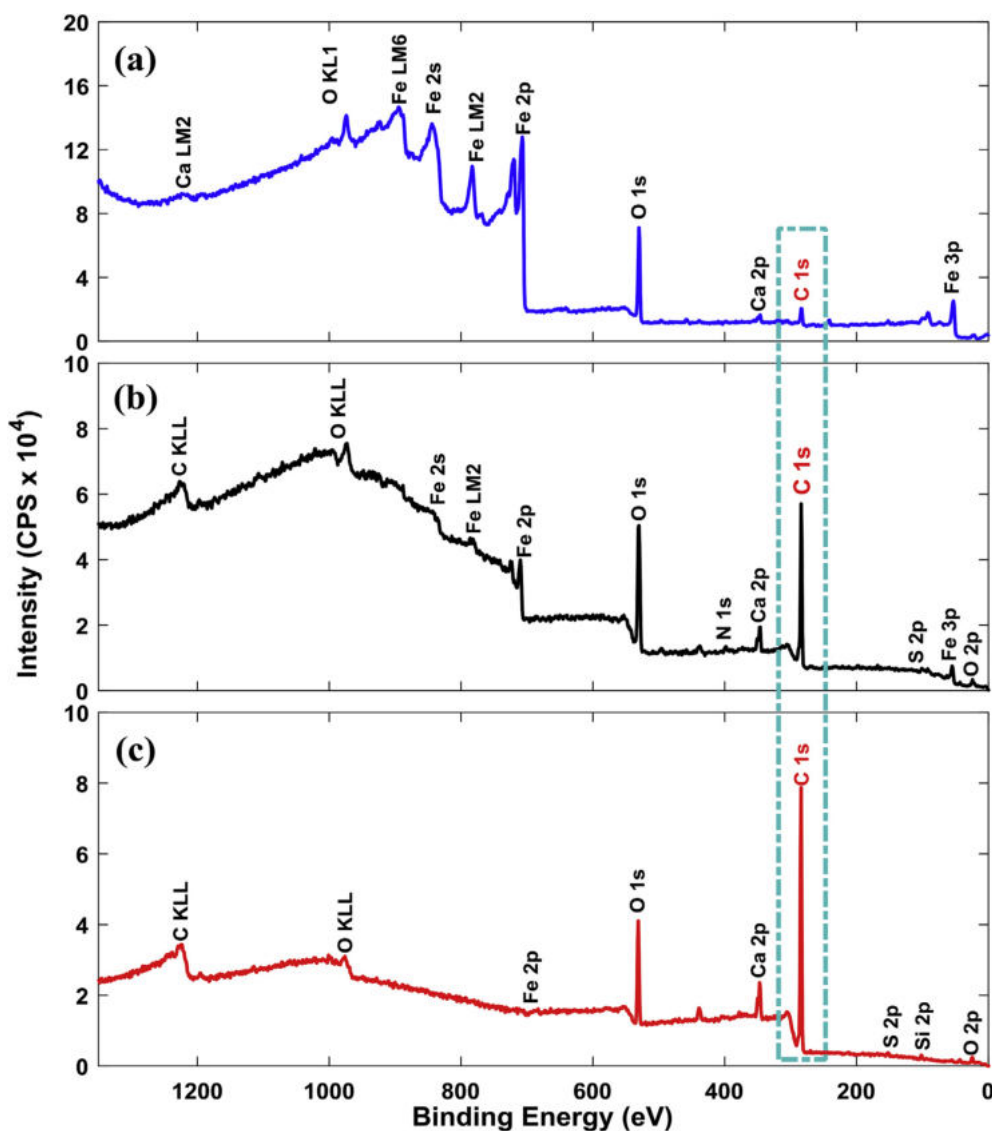
Fig. 20. XPS survey scans of the worn cylinder liner surface. (a) Before friction test, (b) lubricated by reference oil alone and (c) lubricated by Gr nanolubricant.

tribochemical reaction happened during friction process. Fig. 20c confirms the existence of C, originating from the Gr nanolubricant, as well as S, from oil additive package (5W-30). Moreover, Fig. 20c showed the presence of Fe and Si in the tribofilm owing to wear debris from the worn surface. Fe and Si incorporation in the tribofilm composition imply tribofilm is formed due to a chemical reaction of the Gr nanolubricant with the substrate surface with physical adsorption of the Gr nanolubricant on the substrate surface [42].

Fig. 21 shows the high-resolution XPS spectra of the main elements (Fe2p, O and C1s) on the cylinder liner before friction test (Fig. 21a), worn surfaces of the liner lubricated engine oil (Fig. 21b) and worn surfaces of the liner lubricated by Gr nanolubricant (Fig. 21c). In Fig. 21a, C 1s core level spectrum showed a peak at 283.59 eV and this can be attributed to the contaminated carbons from liner surface substrate. The peak of the C 1s at 283.69 eV in Fig. 21b is mainly ascribed to the oxidation of oil additive package and contaminated carbons on the worn surface. Furthermore, the enhanced C=O intensity also demonstrates the probable oxidization of reference oil [24]. However, the C 1s core level spectrum in Fig. 21c is different from the ones in Fig. 21a. The strong peak at 284.19 eV corresponding to the carbon from Gr indicates the existence of the tribofilms on the worn track [43], which matches well with the EDS mapping and line scanning analysis in Figs. 18b and 19. Moreover, the C1s core level spectrum revealed

another peak at 288.8 eV due to different functionalized carbons [44] as shown in Fig. 21c. The spectrum suggests the presence of C=O bond in the tribofilms.

From Fig. 21a, it can be seen that the peak around 529.47 eV is attributed to the O 1s electrons in FeO. As shown in Fig. 21b, the O 1s core-level spectrum present two distinct oxygen contributions corresponding to Fe-O-H and Fe-O-Fe bonds. The O 1s spectra at 530.57 eV is a strong signal from Fe_2O_3 showing oxidation occurred on the worn track during the sliding test lubricated by reference oil (5W-30). Nevertheless, the O 1s core level spectrum of the worn track lubricated by Gr nanolubricant (Fig. 21c), the peak signal at centered around 531.1 eV is indicating a higher oxidation degree of Fe element, which might correspond to Fe_2O_3. From Fig. 21, Fe 2p spectra can be knowing the oxidation extent. Fe 2p spectra in Fig. 21a shows a part of the Fe elements at zero valence state are oxidized to FeO. The Fe 2p core-level spectrum (Fig. 21b) provides two unique peaks located at 709.46 eV and 724 eV corresponding to Fe $2p_{3/2}$ and Fe $2p_{1/2}$, together with two satellite peaks at 717 and 733 eV, respectively. This result proves the iron particles as wear debris was oxidized to Fe_2O_3 under lubricating by engine oil without Gr. Thus, the Fe elements on the worn surface were completely oxidized and transformed to the higher valence state of Fe^{3+} [1]. While, the high-resolution XPS of Fe 2p showed its low contribution in the tribofilm formation with the main form as metal
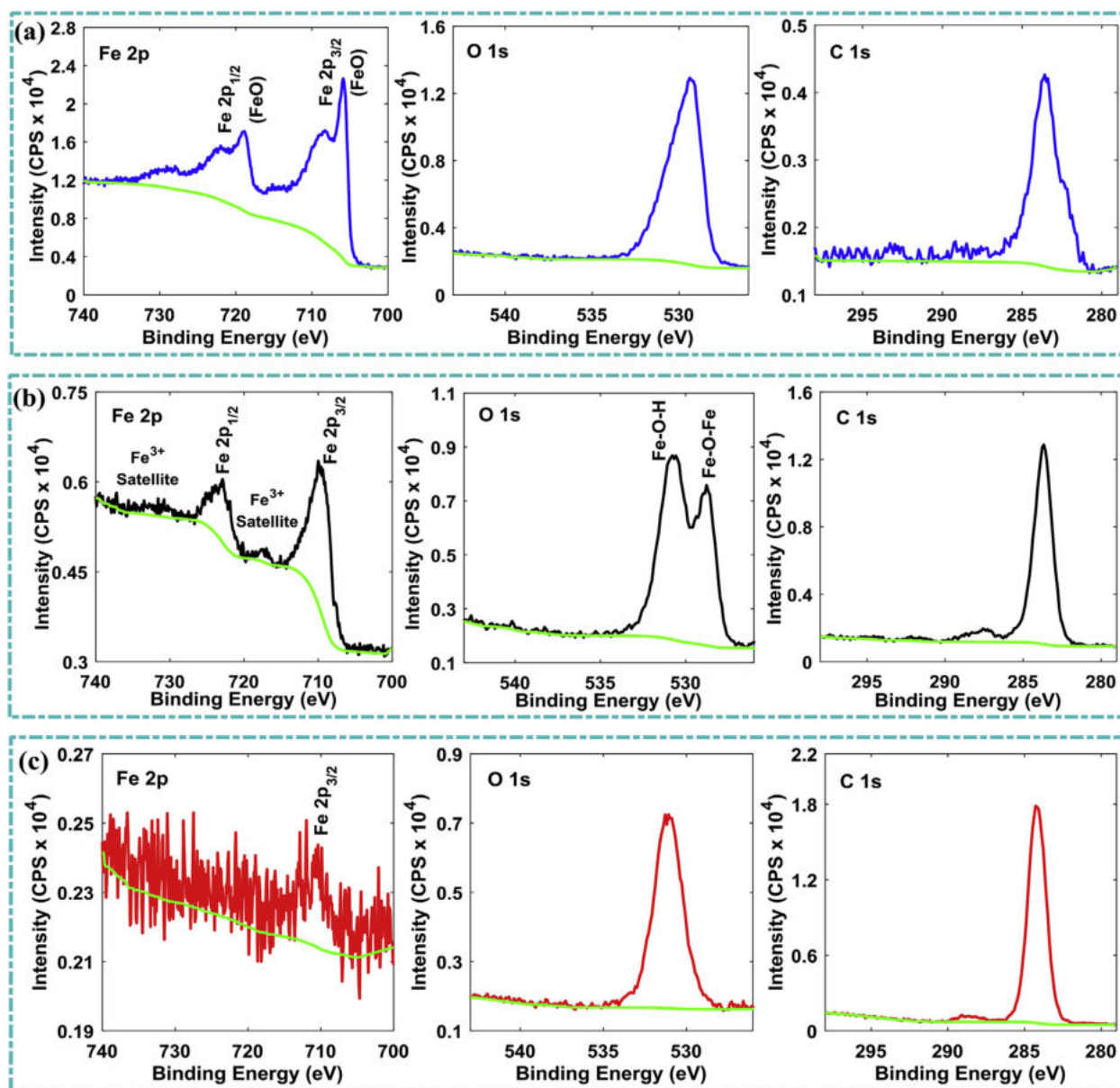
Fig. 21. High-resolution XPS core level spectra of the major elements for cylinder liner. (a) Before friction test, (b) lubricated by reference oil alone and (c) lubricated by Gr nanolubricant.

Table 7
Main elements content of the liner worn surface based on XPS results.

Elements	Before sliding		Reference oil (5W-30)		Gr nanolubricant	
	Peak BE	Atomic %	Peak BE	Atomic %	Peak BE	Atomic %
C 1s	283.59	23.62	283.69	65.61	284.19	80.98
O 1s	529.47	33.36	530.57	29	531.1	15.39
Si 2p	100.8	2.1	–	–	101.43	1.70
Fe 2p	706.41	40.92	709.46	3.88	711.96	0.84
S 2p	–	–	167.15	1.51	162.37	1.09
Total	100	100	100	100	100	100

the substrate surface of the liner and ring (Fe and Si). Additionally, the corresponding atomic percentages and binding energies peak of the main elements in XPS results that contributed to form the self-lubricating films on the worn liner surface are presented in Table 7.

Furthermore, Raman spectroscopy was used to investigate the chemical bonding in the self-lubricating films formed on the rubbing liner surface using Gr nanolubricant. Fig. 22 presented the Raman spectra of the cylinder liner lubricated by Gr nanolubricant compared with the spectra of the cylinder liner lubricated by reference oil. The results showed that the most prominent features in the liner lubricated by Gr nanolubricant so-called G band at around $1582\,\mathrm{cm^{-1}}$ [45], which approve the main contribution of the Gr into self-lubricating films formed on the rubbing liner surface. It is remarkable to say that Raman spectra of the liner lubricated by reference oil presented a characteristic peak of the hematite at $670\,\mathrm{cm^{-1}}$ which matches very well with the reported results of Fe_2O_3 [46]. Additionally, very weak peaks in the range of $1300–1600\,\mathrm{cm^{-1}}$ corresponding to the graphite-like carbon were also observed which prove the carbon not enough for self-lubricating film formation in case of lubrication by reference oil during friction. Based

iron at 711.96 eV as shown in Fig. 21c, which illustrates that the Gr nanolubricant was very effective in the formation self-lubricating films.

According to the EDS elemental maps and XPS characterizations, the major compositions of the self-lubricating protective films on the frictional surfaces were Gr nano-additives (C), organic matters from reference oil and surfactant (C, S, Ca, P and O) and wear oxides from
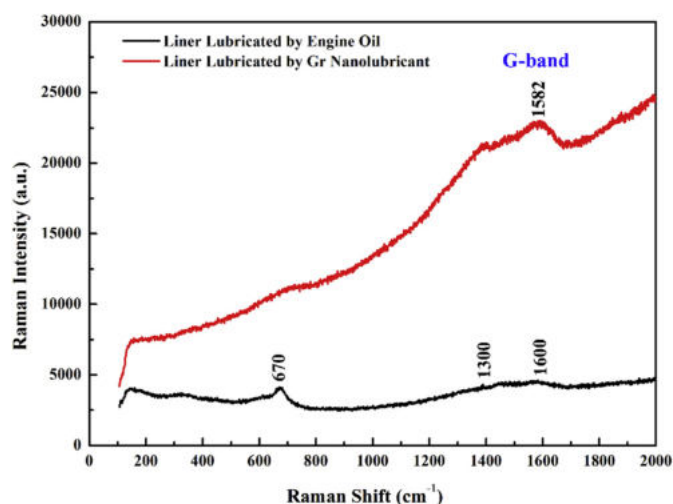
Fig. 22. Raman spectra of the worn cylinder liner surfaces lubricated by reference oil and Gr nanolubricant.

on the XPS and Raman results, the peaks confirm the formation of the self-lubricating layers on the rubbing liner surface as a result of the tribochemical reactions of the Gr nano-additives, liner surface material and oil additive package which is highly consistent with the EDS results.

3.4. Roles of Gr nanolubricant in engine performance and exhaust emissions

The goal of this section is to link tribological tests in the laboratory with factual engine performance during various operating conditions for both reference oil and Gr nanolubricant. Accordingly, the engine characteristics are comparatively presented for the output power, torque, fuel consumption, total frictional power, and emissions (CO, CO_2, HC, and NOx) with respect to different engine speeds and loads. Additionally, fuel consumption was tested in test bench with road load simulation through NEDC.

Fig. 23 dedicates the brake power (BP) and engine torque (Te) (Fig. 23a) for both engine oil (5W-30) and Gr nanolubricant at engine load of 50% and likewise for total frictional power (FP) and fuel consumption (BSFC) (Fig. 23b). The presented engine characteristics (BP,

Te, FP and BSFC) are identical to those of typical trends of gasoline naturally aspirated engine [47]. The brake power trend increased naturalistically as the engine speed grown up due to increase in the number of engine power stroke per time [1,48]. Engine torque is a function of the volumetric efficiency, brake thermal efficiency, calorific value, and fuel-air ratio. Since the time of intake stroke is limited and relatively small in the high-speed ranges, the torque trend decreased as the engine speed increased in which the cylinder volume cannot be fully charged leading to lower volumetric efficiency [49]. What else makes the engine torque behave such a trend is that the frictional losses (negative torque) increased as a function of engine speed, unlike the positive torque that decreased versus engine speeds because the engine is unable to ingest full charge of air at higher speeds.

Fig. 23b compares the experimental results of the FP and BSFC for both 5W-30 engine oil and oil with G additives. Obviously, the FP raise following the speed for both lubrication samples. The reason is that the dominance of hydrodynamic friction at high-speed causes uptick in viscous friction due to the shearing resistance of the oil film [40]. Therefore, engine speed is the major operation parameter that controls the FP. The Gr nanolubricant showed lower FP due to enhancing the tribological characteristics of piston ring assembly, which could reinforce an increase in BP, Te as in the previous results (Fig. 23a). Furthermore, the results exhibited that the BSFC declined as the growth of engine speed till it reaches a minimum value (economic speed zone), and then increases with respect to high engine speeds (over-fueling). This is due to the fact that, at low speeds, the time available for heat to be transferred to cylinder walls is relatively longer per cycle, and allows more heat loss occurs, resulting in lower combustion efficiency [50]. Thus, higher fuel consumption is expected per unit power generated. In the higher speed zones, the BSFC again increases due to higher FP (negative power) and pumping work. The Gr nanolubricant showed the lower BSFC by 4.43–5.61% against the engine oil without Gr nanosheets during various engine speeds.

Fig. 24 shows the fuel economy performance of the Gr nanolubricant that was first demonstrated in the driving cycle (NEDC) comparing commercial oil (5W-30). The NEDC is designed to evaluate the fuel economy of a passenger vehicle by AVL dynamometer with road load simulation. It is observed that fuel consumption for Gr nanolubricant was constantly less than commercial oil (without Gr nano-additives) throughout the urban and motorway roads. Interestingly, the variations of the fueling (fuel consumption) were similar behavior
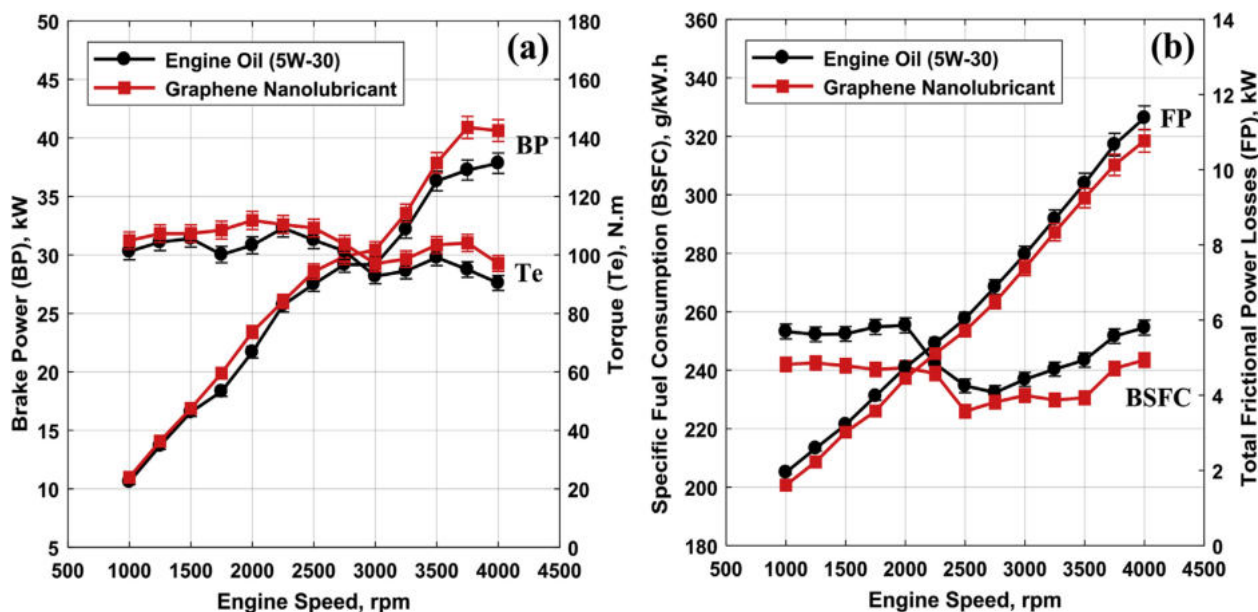

Fig. 23. Engine power, torque, fuel consumption and total frictional power as a function in engine speed rpm.
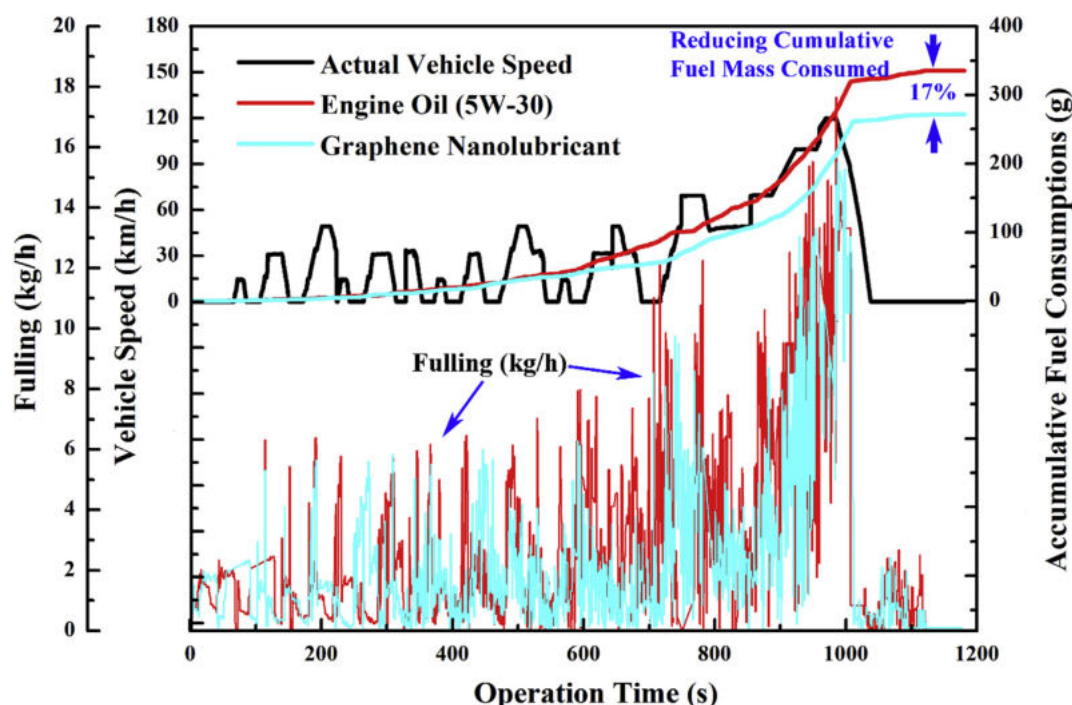
Fig. 24. Fuel consumption obtained during lubrication of the engine by reference oil (5W-30) and Gr nanolubricant under New European Driving Cycle (NEDC).

throughout the NEDC due to the engine characteristics are inter-related with engine loading, but the values of the fueling are different under engine lubrication by commercial oil and Gr nanolubricant. During the urban stages, the engine loading is mainly determined by the vehicle acceleration because of the absolute vehicle speeds are lower, but the transient events both frequent and steep [51]. While, the vehicle speed on the motorway was increased, which most affects the engine loading through an increase of the aerodynamic resistance. Consequently, the fueling peaks increased at high vehicle speeds owing to the power needed to overcome all resistances of the vehicle. In order to show the role of Gr nanolubricant, the cumulative fuel mass consumed during NEDC is plotted in Fig. 24 for comparison between fuel consumption of the commercial oil (5W-30) and Gr nanolubricant under same conditions. The results elucidated that the cumulative fuel mass using Gr nanolubricant is lower than commercial oil (5W-30).

In summary, the BP and Te results corresponding to the Gr nanolubricant increased by 7–10%, against the lube oil without Gr additives. The reason for BP and Te enhancement is due to lower FP by 6% in the case of Gr nanolubricant. Notably in eventually, the Gr nanolubricant enhanced the fuel economy in which up to 17% reducing cumulative fuel mass consumed against the commercial oil (5W-30) during NEDC. This is related to the decline of the friction and wear of the piston ring assembly in the engine resulting anti-friction and anti-wear as shown in Figs. 9–11. The principal reason for improving anti-friction and anti-wear is the formation rate of a tribofilm from Gr nanolubricant greater than the film removal rate from worn surfaces as well as a strong adhesion and cohesion with substrate surfaces in the engine as explained in Section 3.3.

Further information of the influence of the Gr nanolubricant on the exhaust emissions (CO_2, HC, CO, and NO_X) comparing with reference oil (5W-30) was evaluated through various engine speeds and loads. Fig. 25 displays the comparison between the emissions generated during engine lubrication by the commercial oil (5W-30) and Gr nanolubricant. Generally, CO_2 is non-toxic but contributes to the greenhouse effect [52]. Fig. 25a presented the effect of the engine speed with different throttle valve positions on the CO_2 during lubrication engine by Gr nanolubricant compared with reference oil. The results show a reduction by 3.4–4.66% in the CO_2 emissions obtained with the Gr

nanolubricant compared with reference oil under various engine speeds and different throttle valve openings. Moreover, the fuel consumption reduction reflects on a lower CO_2 emissions during engine lubrication by Gr nanolubricant. Generally speaking, it can be said that the trend in fuel consumption and CO_2 emissions present exactly the same trend. According to the comparison of the similar experimental studies and the current study, the Gr nanolubricant presented the reduction in the CO_2 emissions with fuel economy more than the results obtained by other researchers [36,53].

Whilst, CO is a harmful and dangerous gas, it is important to reduce its level of emissions in automobile engines [54]. Fig. 25b presents the variation of CO with the engine speeds under various throttle valve openings for both the lubricant oils. The results display that the CO with throttle valve openings of 50% increases when engine speed increases until it reaches a 2500 rpm, and then decreases after 3000 rpm engine speed. This is due to the fact that, at high engine speeds, the exhaust temperature and also turbulence in the combustion chamber were increased resulting in complete combustion due to suppressing the oxidation process even though sufficient oxygen would be for combustion [55]. In fact, it can be seen that no systematic trend of CO values was observed under lubrication by engine oil or Gr nanolubricant. As demonstrated in Fig. 25c, it is found that HC for both the lubricant oils decreased with increasing engine speed during throttle valve opening of 75% until it reaches a 2500 rpm and then slightly increases with high engine speed. However, during throttle valve opening of 50% for both lubricant oils, HC also decreased until it reaches a 2000 rpm and then increases with increasing engine speeds. As a general trend, the HC was reduced during engine lubrication by Gr nanolubricant, as compared to reference oil especially under high engine loads (75% throttle valve opening). The reason for the decrease in HC with the higher engine loads is the higher temperatures of the exhaust flue gases [56]. The effect of Gr nanolubricant is also evident in terms of NO_X (Fig. 25d), where the engine out emissions are greater with respect to the base oil, at all investigated engine speeds. It can say that the use of Gr nanolubricant reduced the NO_X by approximately 3–5%, especially at low-speed operation when exhaust temperature may not be sufficient for NOx reduction.

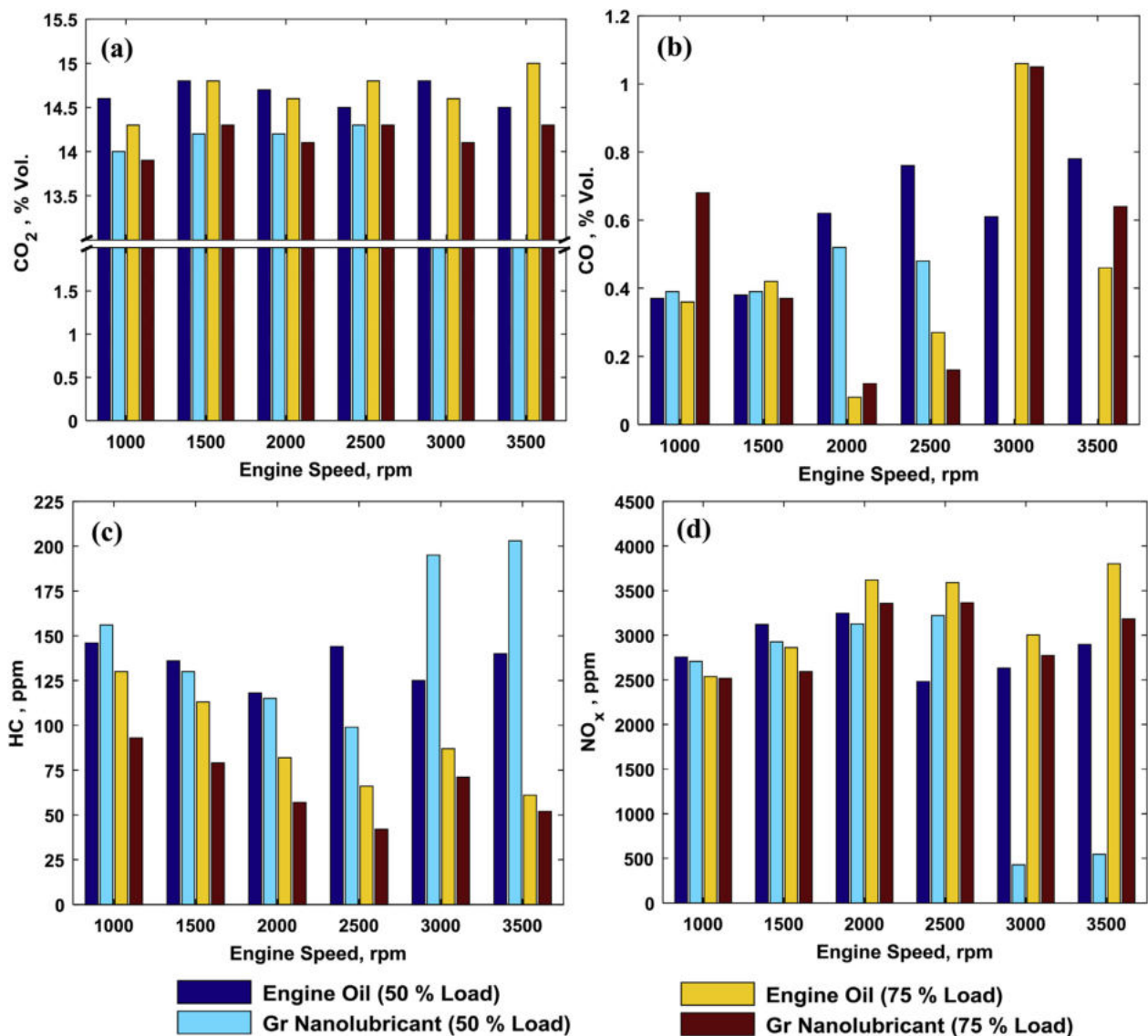Based on the obtained results in Figs. 24 and 25, it can be concluded

Fig. 25. The effect of the Gr nanolubricant on the exhaust emissions (CO_2, HC, CO, and NO_X) under various operating conditions.

that the Gr nanolubricant provide a straightforward approach to automotive fuel economy and reduce the exhaust emissions down to levels even lower than in the case of reference oil (5W-30) under most operating conditions. This is due to the positive impacts of the self-lubricating layers (tribofilms) formed on the piston ring and cylinder liner from Gr nanolubricant as presented in Section 3.3, which enhanced heat transfer because of the high thermal conductivity of the Gr. As known, the operating temperatures of the cylinder liner is an important factor affecting HC and NOx emissions. For instance, the NOx emissions tend to be reduced with a lower liner temperature, whilst the HC emissions tend to be reduced with a high liner temperature [57,58]. Accordingly, an optimum liner temperature should be explored, based upon a wanted trade-off between the NOx and HC emissions during engine lubrication by nanolubricant. Furthermore, the self-lubricating layers on the cylinder liner and piston ring were attributed for helping in the increase of the cylinder pressure arising from combustion owing to increase of the sealing between the ring and liner, which reduces also the blow-by gases. Further investigation will be required to present the mechanisms responsible for the reduction of the exhaust emissions by nanolubricant additives.

4. Conclusions

The friction and wear are responsible for the power losses during engine operation, leading to an increased fuel consumption and ultimately increased emissions. Therefore, this study contributes saving energy in automobile engines via self-healing mechanism of the engine worn surfaces using Gr nanolubricant to support anti-friction/wear properties, especially under boundary lubrication regime. Based on the results and discussion, the main conclusions can be drawn from this study as follows:

1 The tribological tests presented that the anti-friction and anti-wear properties improved in the range 29–35% and 22–29%, respectively, with the worn surfaces lubricated by Gr nanolubricant under running conditions involving boundary lubrication regime, as compared to the reference oil (5W-30). The principal reason responsible for anti-friction and anti-wear is self-healing mechanism by formation of Gr tribofilms on the worn surfaces as exhibited in morphologies tests by FE-SEM, EDS, 3D surface roughness profile, Raman and XPS tests.

2 The experimental results using an AVL dynamometer under various engine loads and speeds indicated that the engine performance

improved during engine lubrication by Gr nanolubricant. Consequently, the actual engine power and torque increased by 7–10% due to lower total frictional power by 6% as a direct result of improving the anti-friction and anti-wear.

3 The lubrication of the engine using Gr nanolubricant achieves 17% reduction in the consumed cumulative fuel mass with road load simulation by AVL dynamometer using the New European Driving Cycle (NEDC).

4 The exhaust emissions results showed that CO_2, HC and NOx gaseous decreased by 2.79–5.42% when the engine lubricated by Gr nanolubricant. The modest decrease in NOx emissions was due to lower combustion temperature caused by improving the heat transfer through tribofilms formed on the cylinder liner.

Further investigations should answer the question of what are the mechanisms responsible for the reduction of the exhaust emissions by nanolubricant additives. Furthermore, further investigations are needed to study the effect of the hybrid nanolubricants, which helps to further the reduction of the emissions from automobile engines, especially at the cold start.

Conflict of interest

The authors declare no competing financial interest.

Acknowledgments

References

[1] Ali MKA, Fuming P, Younus HA, Abdelkareem MAA, Essa FA, Elagouz A, Xianjun H. Fuel economy in gasoline engines using Al_2O_3/TiO_2 nanomaterials as nanolubricant additives. Appl Energy 2018;211:461–78.

[2] Xiao H, Liu S. 2D nanomaterials as lubricant additive: a review. Mater Des 2017;135:319–32.

[3] Ali MKA, Xianjun H. Improving the tribological behavior of internal combustion engines via the addition of nanoparticles to engine oils. Nanotechnol Rev 2015;4:347–58.

[4] Hisham S, Kadirgama K, Ramasamy D, Noor MM, Amirruddin AK, Najafi G, Rahmana MM. Waste cooking oil blended with the engine oil for reduction of friction and wear on piston skirt. Fuel 2017;205:247–61.

[5] Ali MKA, Xianjun H, Essa FA, Abdelkareem MAA, Elagouz A, Sharshir SW. Friction and wear reduction mechanisms of the reciprocating contact interfaces using nanolubricant under different loads and speeds. ASME J Tribol 2018. http://dx.doi.org/10.1115/1.4039720.

[6] Tung SC, McMillan ML. Automotive tribology overview of current advances and challenges for the future. Tribol Int 2004;37:517–36.

[7] Liu J, Zheng Z, Li F, Lei W, Gao Y, Wu Y, et al. Nanoparticle chemically end-linking elastomer network with super-low hysteresis loss for fuel-saving automobile. Nanomater Energy 2016;28:87–96.

[8] Ali MKA, Xianjun H, Elagouz A, Essa FA, Abdelkareem MAA. Minimizing of the boundary friction coefficient in automotive engines using Al_2O_3 and TiO_2 nanoparticles. J Nanoparticle Res 2016;18:377.

[9] Ali MKA, Xianjun H, Mai L, Bicheng C, Turkson RF, Qingping C. Reducing frictional power losses and improving the scuffing resistance in automotive engines using hybrid nanomaterials as nano-lubricant additives. Wear 2016;364–365:270–81.

[10] Rasheed AK, Khalid M, Javeed A, Rashmi W, Gupta TCSM, Chan A. Heat transfer and tribological performance of graphene nanolubricant in an internal combustion engine. Tribol Int 2016;103:504–15.

[11] Ali MKA, Xianjun H, Mai L, Qingping C, Turkson RF, Bicheng C. Improving the tribological characteristics of piston ring assembly in automotive engines using Al_2O_3 and TiO_2 nanomaterials as nano-lubricant additives. Tribol Int 2016;103:540–54.

[12] Joly-Pottuz L, Ohmae N. Carbon-based nanolubricants. John Wiley & Sons, Ltd; 2008. p. 93–147. Nanolubricants.

[13] Ali MKA, Xianjun H, Turkson RF, Peng Z, Chen X. Enhancing the thermophysical properties and tribological behaviour of engine oils using nano-lubricant additives. RSC Adv 2016;6:77913–24.

[14] Zhang W, Demydov D, Jahan MP, Mistry K, Erdemir A, Malshe AP. Fundamental understanding of the tribological and thermal behavior of Ag–MoS_2 nanoparticle-based multi-component lubricating system. Wear 2012;288:9–16.

[15] Ratoi M, Niste VB, Alghawel H, Suen YF, Nelson K. The impact of organic friction modifiers on engine oil tribofilms. RSC Adv 2014;4:4278–85.

[16] Jeng Y-R, Huang Y-H, Tsai P-C, Hwang G-L. Tribological performance of oil-based lubricants with carbon-fe nanocapsules additive. Tribol Trans 2015;58:924–9.

[17] Yang J, Zhang H, Chen B, Tang H, Li C, Zhang Z. Fabrication of the g-C_3N_4/Cu nanocomposite and its potential for lubrication applications. RSC Adv 2015;5:64254–60.

[18] Rajendhran N, Palanisamy S, Periyasamy P, Venkatachalam R. Enhancing of the tribological characteristics of the lubricant oils using Ni-promoted MoS_2 nanosheets as nano-additives. Tribol Int 2018;118:314–28.

[19] Wu H, Wang L, Johnson B, Yang S, Zhang J, Dong G. Investigation on the lubrication advantages of MoS_2 nanosheets compared with ZDDP using block-on-ring tests. Wear 2018;394–395:40–9.

[20] Cheng Z-L, Li W, Wu P-R, Liu Z. Study on structure-activity relationship between size and tribological properties of graphene oxide nanosheets in oil. J Alloy Comp 2017;722:778–84.

[21] Fan X, Li W, Fu H, Zhu M, Wang L, Cai Z, et al. Probing the function of solid nanoparticle structure under boundary lubrication. ACS Sustain Chem Eng 2017;5:4223–33.

[22] Guzman Borda FL, Ribeiro de Oliveira SJ, Seabra Monteiro Lazaro LM, Kalab Leiróz AJ. Experimental investigation of the tribological behavior of lubricants with additive containing copper nanoparticles. Tribol Int 2018;117:52–8.

[23] Wu H, Zhao J, Cheng X, Xia W, He A, Yun J-H, et al. Friction and wear characteristics of TiO2 nano-additive water-based lubricant on ferritic stainless steel. Tribol Int 2018;117:24–38.

[24] Meng Y, Su F, Chen Y. Au/graphene oxide nanocomposite synthesized in supercritical co_2 fluid as energy efficient lubricant additive. ACS Appl Mater Interfaces 2017;9:39549–59.

[25] Rashmi W, Khalid M, Xiao Y, GUPTA TCSM AG. Tribological studies on graphene/TEM based nanolubricant. J Eng Sci Technol 2017;12:365–73.

[26] Chou R, Battez AH, Cabello JJ, Viesca JL, Osorio A, Sagastume A. Tribological behavior of polyalphaolefin with the addition of nickel nanoparticles. Tribol Int 2010;43:2327–32.

[27] Yu HL, Xu Y, Shi PJ, Xu BS, Wang XL, Liu Q, Wang HM. Characterization and nanomechanical properties of tribofilms using Cu nanoparticles as additives. Surf Coating Technol 2008;203:28–34.

[28] Ingole S, Charanpahari A, Kakade A, Umare SS, Bhatt DV, Menghani J. Tribological behavior of nano TiO_2 as an additive in base oil. Wear 2013;301:776–85.

[29] Sgroi MF, Asti M, Gili F, Deorsola FA, Bensaid S, Fino D, et al. Engine bench and road testing of an engine oil containing MoS2 particles as nano-additive for friction reduction. Tribol Int 2017;105:317–25.

[30] Skjoedt M, Butts R, Assanis DN, Bohac SV. Effects of oil properties on spark-ignition gasoline engine friction. Tribol Int 2008;41:556–63.

[31] Tormos B, Ramírez L, Johansson J, Björling M, Larsson R. Fuel consumption and friction benefits of low viscosity engine oils for heavy duty applications. Tribol Int 2017;110:23–34.

[32] Choi H-J, Jung S-M, Seo J-M, Chang DW, Dai L, Baek J-B. Graphene for energy conversion and storage in fuel cells and supercapacitors. Nanomater Energy 2012;1:534–51.

[33] Erdemir A, Ramirez G, Eryilmaz OL, Narayanan B, Liao Y, Kamath G, et al. Carbon-based tribofilms from lubricating oils. Nature 2016;536:67–71.

[34] Berman D, Erdemir A, Sumant AV. Approaches for achieving superlubricity in two-dimensional materials. ACS Nano 2018. http://dx.doi.org/10.1021/acsnano.7b09046.

[35] Low SS, Loh H-S, Boey JS, Khiew PS, Chiu WS, Tan MTT. Sensitivity enhancement of graphene/zinc oxide nanocomposite-based electrochemical impedance genosensor for single stranded RNA detection. Biosens Bioelectron 2017;94:365–73.

[36] Sgroi M, Asti M, Gili F, Deorsola FA, Bensaid S, Fino D, Kraft G, Garcia I, Dassenoy F. Engine bench and road testing of an engine oil containing MoS_2 particles as nano-additive for friction reduction. Tribol Int 2017;105:317–25.

[37] Derjaguin BV, Churaev NV, Muller VM. The derjaguin-landau-verwey-overbeek (DLVO) theory of stability of lyophobic colloids. Surface Forces. Boston, MA: Springer US; 1987. p. 293–310.

[38] Morina A, Lee P, Priest M, Neville A. Challenges of simulating 'fired engine'ring-liner oil additive/surface interactions in ring-liner bench tribometer. Tribol Mater Surface Interfac 2011;5:25–33.

[39] Hamrock D, Dowson D. Ball bearing lubrication: the elastohydrodynamics of elliptical contacts. New York: Wiley; 1981.

[40] Ali MKA, Xianjun H, Turkson RF, Ezzat M. An analytical study of tribological parameters between piston ring and cylinder liner in internal combustion engines. Proc Inst Mech Eng Part K J Multi-body Dyn 2016;230:329–49.

[41] Wan S, Tieu AK, Xia Y, Wang L, Li D, Zhang G, et al. Tribochemistry of adaptive integrated interfaces at boundary lubricated contacts. Sci Rep 2017;7. 9935.

[42] Willermet P, Dailey D, Carter R, Schmitz P, Zhu W. Mechanism of formation of antiwear films from zinc dialkyldithiophosphates. Tribol Int 1995;28:177–87.

[43] Zhu Y, Murali S, Stoller MD, Ganesh K, Cai W, Ferreira PJ, et al. Carbon-based supercapacitors produced by activation of graphene. Science 2011;332:1537–41.

[44] Jaiswal V, Umrao S, Rastogi RB, Kumar R, Srivastava A. Synthesis, characterization,

and tribological evaluation of tio$_2$-reinforced boron and nitrogen co-doped reduced graphene oxide based hybrid nanomaterials as efficient antiwear lubricant additives. ACS Appl Mater Interfaces 2016;8:11698–710.

[45] Rasheed A, Khalid M, Rashmi W, Gupta T, Chan A. Graphene based nanofluids and nanolubricants–Review of recent developments. Renew Sustain Energy Rev 2016;63:346–62.

[46] Genchev G, Erbe A. Raman spectroscopy of mackinawite FeS in anodic iron sulfide corrosion products. J Electrochem Soc 2016;163:C333–8.

[47] Mourad M, Mahmoud KR. Performance investigation of passenger vehicle fueled by propanol/gasoline blend according to a city driving cycle. Inside Energy 2018;149:741–9.

[48] Etsion I, Sher E. Improving fuel efficiency with laser surface textured piston rings. Tribol Int 2009;42:542–7.

[49] Alahmer A. Influence of using emulsified diesel fuel on the performance and pollutants emitted from diesel engine. Energy Convers Manag 2013;73:361–9.

[50] Heywood JB. Internal combustion engine fundamentals. New York: Mcgraw-Hill; 1988.

[51] Giakoumis EG, Zachiotis AT. Comparative evaluation of eight legislated driving schedules in terms of cycle metrics and emissions from a diesel-powered turbo-charged van. Transport Res Transport Environ 2018;58:139–54.

[52] Marotta A, Pavlovic J, Ciuffo B, Serra S, Fontaras G. Gaseous emissions from light-duty vehicles: moving from NEDC to the new WLTP test procedure. Environ Sci Technol 2015;49:8315–22.

[53] Vittorini D, Di Battista D, Cipollone R. Engine oil warm-up through heat recovery on exhaust gases–emissions reduction assessment during homologation cycles. Therm Sci Eng Prog 2018;5:412–21.

[54] Turkson RF, Yan F, Ali MKA, Liu B, Hu J. Modeling and multi-objective optimization of engine performance and hydrocarbon emissions via the use of a computer aided engineering code and the NSGA-II genetic algorithm. Sustainability 2016;8:72.

[55] Ghazikhani M, Hatami M, Safari B, Domiri Ganji D. Experimental investigation of exhaust temperature and delivery ratio effect on emissions and performance of a gasoline–ethanol two-stroke engine. Case Stud Therm Eng 2014;2:82–90.

[56] Castillo Marcano SJ, Bensaid S, Deorsola FA, Russo N, Fino D. Nanolubricants for diesel engines: related emissions and compatibility with the after-treatment catalysts. Tribol Int 2014;72:198–207.

[57] Arapatsakos CKA, Strofylla SM. The effect of temperature on gas emissions. IJRRAS 2012;11:89–100.

[58] Rahmani R, Rahnejat H, Fitzsimons B, Dowson D. The effect of cylinder liner operating temperature on frictional loss and engine emissions in piston ring conjunction. Appl Energy 2017;191:568–81.